

Higgs production in association with a top-antitop pair in the Standard Model Effective Field Theory at NLO in QCD

Fabio Maltoni,^a Eleni Vryonidou^a and Cen Zhang^b

^a*Centre for Cosmology, Particle Physics and Phenomenology (CP3),
Université catholique de Louvain, B-1348 Louvain-la-Neuve, Belgium*

^b*Department of Physics, Brookhaven National Laboratory, Upton, NY 11973, USA*

E-mail: fabio.maltoni@uclouvain.be, eleni.vryonidou@uclouvain.be,
cenzhang@bnl.gov

ABSTRACT: We present the results of the computation of the next-to-leading order QCD corrections to the production cross section of a Higgs boson in association with a top-antitop pair at the LHC, including the three relevant dimension-six operators ($O_{t\varphi}$, $O_{\varphi G}$, O_{tG}) of the standard model effective field theory. These operators also contribute to the production of Higgs bosons in loop-induced processes at the LHC, such as inclusive Higgs, Hj and HH production, and modify the Higgs decay branching ratios for which we also provide predictions. We perform a detailed study of the cross sections and their uncertainties at the total as well as differential level and of the structure of the effective field theory at NLO including renormalisation group effects. Finally, we show how the combination of information coming from measurements of these production processes will allow to constrain the three operators at the current and future LHC runs. Our results lead to a significant improvement of the accuracy and precision of the deviations expected from higher-dimensional operators in the SM in both the top-quark and the Higgs-boson sectors and provide a necessary ingredient for performing a global EFT fit to the LHC data at NLO accuracy.

Contents

1	Introduction	1
2	Effective operators	4
3	Calculation setup	7
4	Theoretical uncertainties	8
5	Numerical results	11
5.1	Total cross sections	11
5.2	Distributions	17
6	RG effects	23
7	Constraints on dimension-six operators	26
8	Summary and conclusions	32

1 Introduction

The top quark and the Higgs boson are the two heaviest elementary particles known to date. Their interaction is expected to reveal evidence of beyond the standard model (SM) physics and possibly determine the fate of the universe [1]. The LHC provides us the first chance to measure the interactions of these two particles through the associated production of a Higgs with a single top quark [2–4] or a top quark pair [5–14]. At the LHC, precise measurements require accurate input from the theory side. Predictions for the $t\bar{t}H$ process in the SM are known at next-to-leading order (NLO) in QCD [15–22], with off-shell effects [23], and at NLO in electroweak [24–27]. Next-to-leading logarithmic matched to NLO [28] as well as approximate next-to-next-to-leading order QCD predictions [29] have also become available recently.

In addition to the SM prediction, we expect that a precise understanding of the patterns of deviations from the SM will become equally important at the LHC Run II, given the complicated nature of the corresponding measurements [30–35], and the attainable precision on the top-quark couplings expected for Run II measurements [36]. A powerful and predictive framework to analyse possible deviations is provided by the SM effective field theory (SMEFT) [37–39], i.e. the SM augmented by higher-dimensional operators. In this framework, radiative corrections to the SM deviations can be consistently included in a model-independent way, thus allowing for systematically improving the predictions. In fact, NLO corrections for a set of top-quark processes have recently started to become

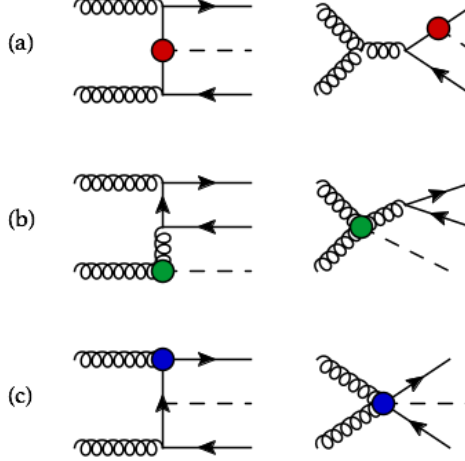


Figure 1. Example diagrams for $t\bar{t}H$ production. The inserted operators are: (a) $O_{t\varphi}$ (b) $O_{\varphi G}$ (c) O_{tG} .

available in such a framework, including top-quark decay processes, flavor-changing neutral production, top-pair production, single-top production, and $t\bar{t}$ associated production with a Z -boson and with a photon [40–47]. Several Higgs decay results have also become available recently [48–51].

The goal of this work is to improve the predictions of such deviations in $t\bar{t}H$ production in SMEFT by computing the NLO QCD corrections. Besides, we will also present SMEFT results for processes that are top-loop induced in the SM, such as $pp \rightarrow H$, $pp \rightarrow Hj$ and Higgs pair production $pp \rightarrow HH$. Selected Feynman diagrams at the leading order (LO) are shown in Figure 1 and 2 for the $t\bar{t}H$ and loop-induced processes, respectively. The relevant effective operators in these processes, i.e. those modifying ttH , ttg , and ggH vertices, are both physically interesting and practically important, because they connect the top-quark sector with the Higgs-boson sector in the SMEFT at dimension-six. Studying these processes and interactions will allow us to investigate how much we can learn about the top quark from Higgs measurements, and vice versa. In particular, the chromo-magnetic dipole operator O_{tG} , which gives rise to a dipole interaction in the $g\bar{t}t$ vertex and introduces $gg\bar{t}t$, $g\bar{t}tH$, and $gg\bar{t}tH$ vertices, is often left out in Higgs operator analyses (see, for example, [52–60]), because it is often considered as part of top-quark measurements. Here we will show that the current $t\bar{t}H$ and $pp \rightarrow H$ measurements already provide useful information about the chromo-dipole moment, comparable to what we can learn from top-pair production, and that future measurements will improve the limits. This observation implies that Higgs measurements are becoming sensitive to this interaction and therefore it should not be neglected. Furthermore, the extraction of the Higgs self-coupling from $pp \rightarrow HH$ measurements relies on a precise knowledge of the top-Higgs interactions. Here we compute for the first time the contribution from the chromo-dipole moment O_{tG} to Higgs pair production. As it will be shown in the following, this operator gives a large contribution to this process, even taking into account the current constraints from $t\bar{t}$ production on the

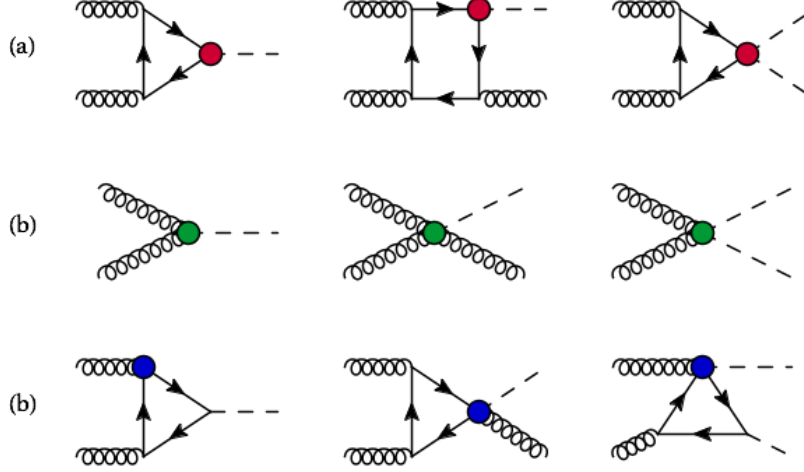


Figure 2. Example diagrams for H , Hj , and HH production. The inserted operators are: (a) $O_{t\varphi}$ (b) $O_{\varphi G}$ (c) O_{tG} . LO contributions from $O_{\varphi G}$ are at the tree level, while those from the other two operators are induced by a top-quark loop.

size of its coefficient.

Let us briefly discuss the motivations for having NLO SMEFT predictions.

- First, the impact of QCD corrections on the central values, which can be conventionally estimated by a K factor (the ratio of NLO central prediction to LO), is often large at the LHC, and for an inclusive measurement this will improve the exclusion limit on the effective operators. In addition, NLO corrections improve not only the accuracy of the predictions by modifying the central value, but also the precision by reducing the theoretical uncertainties due to missing higher-order corrections, which leads to a further improvement on the limits. For example, the current limit on the chromo-magnetic dipole operator from $t\bar{t}$ is improved by a factor of 1.5 by including QCD corrections [43], and the effects are even larger in the flavor-changing neutral sector [42, 61–65].
- Second, QCD corrections often change the distributions due to effective operators in a nontrivial way, not captured by the LO scale uncertainty. As the distribution measurements start to play an important role in the EFT global analyses both in the top-quark and in the Higgs sector [57–60, 66, 67], reliable predictions for the distributions are needed as theory inputs. In fact, Ref. [44] has shown that in an operator fit, missing QCD corrections to the shapes could lead to a biased interpretation in terms of new physics models. For this reason our final goal is to use the NLO predictions in a global EFT fit, including differential measurements, to extract maximal information on the operator coefficients.
- Third, unlike in the SM where all the gauge couplings are known, the SMEFT has many operator coefficients, and several of them remain to be constrained. Higher order effects are important in that respect as they can be enhanced by the ratio of

two operator coefficients, C_2/C_1 , if operator O_1 contributes at the tree level, while O_2 at the loop level, and if C_2 is loosely constrained. An example is $gg \rightarrow H$, where at the tree level only the operator $O_{\phi G}$ (corresponding to a ggH vertex) enters, but at the loop level additional operators, for example the $O_{t\phi}$ which shifts the SM top Yukawa coupling, will come in through a top loop. The process can be then used to determine the top Yukawa through a top-loop effect. Similar loop-induced scenarios have been used to obtain information on many other operators (see, for example, [68–74]). Even though this is not particularly relevant in the $t\bar{t}H$ process, the same tree/loop degeneracy in the ggH and the $t\bar{t}H$ vertices will occur, and having NLO corrections allow us to control these effects.

- Fourth, NLO is important to understand the structure of the effective theory, mainly because of the renormalisation group (RG) and operator mixing effects [75–77], and the corresponding theoretical uncertainties due to missing higher-order terms, which we will discuss in this work. At NLO we start to have control on these effects. Furthermore, it is often the case that new operators enter when certain processes are considered at NLO.
- Finally, in the future, the sensitivity of measurements to the effective deviations may be improved, by making use of the accurate EFT predictions and designing optimised experimental strategies in a top-down way. However, given that any useful predictions at the LHC must be at least at NLO, possibly with parton shower (PS) simulation, this improvement will be difficult without a consistent EFT at NLO prediction.

As discussed also in our previous work, an important feature of our computation is that NLO predictions matched to the parton shower can be obtained in an automatic way. The results we will provide are important not only because predictions are improved in accuracy and in precision, but also because NLO+PS event generation can be directly used in an experimental simulation, allowing for a more dedicated investigation of potential deviations, with possibly optimised selections and improved sensitivities to EFT signals. Our approach is based on the MADGRAPH5_AMC@NLO (MG5_AMC) framework [78], and is part of the ongoing efforts of automating NLO EFT simulations for colliders [79].

This paper is organised as follows. In Section 2, we discuss the operators used in this work, while in Section 3 we present our calculation setup. Section 4 is dedicated to a discussion of the relevant theoretical uncertainties. Section 5 presents our results for the total cross sections and differential distributions, and in Section 6 we discuss RG effects relevant for our study. Finally, in Section 7 we obtain constraints on the dimension-six operators using LHC results before we conclude in Section 8.

2 Effective operators

In an EFT approach, potential deviations from the SM can be consistently and systematically described by adding higher-dimensional operators of the SM fields. By employing global analyses [66, 67, 80], experimental results can be used to determine the size of the

deviations due to each effective operator. The established deviations can then be consistently evolved up to high scales, and matched to possible new physics scenarios. In the absence of convincing evidence for new resonance states¹, the SMEFT provides the most model-independent approach to a global interpretation of measurements.

The Lagrangian of SMEFT can be written as

$$\mathcal{L}_{\text{EFT}} = \mathcal{L}_{\text{SM}} + \sum_i \frac{C_i}{\Lambda^2} O_i + \mathcal{O}(\Lambda^{-4}) + h.c., \quad (2.1)$$

where Λ is the scale of new physics. In the $t\bar{t}H$ production there are two kinds of relevant operators: those with four fermion fields and those with two or no fermion fields. The main focus of this work is on the second kind, including the following three operators:

$$O_{t\phi} = y_t^3 \left(\phi^\dagger \phi \right) (\bar{Q}t) \tilde{\phi}, \quad (2.2)$$

$$O_{\phi G} = y_t^2 \left(\phi^\dagger \phi \right) G_{\mu\nu}^A G^{A\mu\nu}, \quad (2.3)$$

$$O_{tG} = y_t g_s (\bar{Q} \sigma^{\mu\nu} T^A t) \tilde{\phi} G_{\mu\nu}^A. \quad (2.4)$$

Our convention is such that for each operator we will add its Hermitian conjugate, even if it is already Hermitian. We assume $C_{t\phi}$ and C_{tG} are real, so that the Lagrangian respects the CP symmetry. $C_{\phi G}$ is always real because the operator is Hermitian. We do not include the CP-odd $O_{\phi\tilde{G}}$ operator. In this work we focus on these three operators². The first one rescales the top Yukawa coupling in the SM, and also gives rise to a new $t\bar{t}HH$ coupling which contributes to Higgs pair production. The third one represents the chromo-dipole moment of the top quark. It modifies the $g\bar{t}t$ vertex in the SM and produces new four-point vertices, $gg\bar{t}t$ and $g\bar{t}tH$, as well as a five-point $gg\bar{t}tH$ vertex. The second one is a loop-induced interaction between the gluon and Higgs fields. Even though it does not involve a top-quark field explicitly, it needs to be included for consistency, in particular at NLO, because the O_{tG} mixes into this operator, and this operator in addition mixes into $O_{t\phi}$, through RG running. All three operators contribute to the $t\bar{t}H$ process at the tree level. In addition, they can also be probed by H , Hj , and HH production processes, where $O_{\phi G}$ contributes at the tree level while the other two contribute at the loop level. In particular, the degeneracy in $gg \rightarrow H$ between the tree/loop-level contributions from $O_{\phi G}$ and $O_{t\phi}$ has been discussed in the context of Hj [82–84] and HH production [85]. We note here that the Higgs pair production involves additional operators that modify the Higgs self coupling. We do not include those here as the QCD part factorises and their effect has been extensively discussed in the literature [86–89]. Rather, we focus on the top-quark operators, in particular O_{tG} , which has not been considered in previous SMEFT analyses.

We normalise these operators so that their tree level contributions to the $pp \rightarrow t\bar{t}H$ cross section are of the same order $[O(\alpha_s^2\alpha)]^3$. Then we can define the “NLO QCD” corrections, i.e. higher-order contributions at $O(\alpha_s^3\alpha)$. In addition, with this parametrisation,

¹A generic EFT might be useful also in the presence of new resonances, see for example [81].

²The operator $O_{\varphi\Box} = (\varphi^\dagger\varphi)\Box(\varphi^\dagger\varphi)$ also contributes by universally rescaling the Higgs couplings. We omit it here because the NLO corrections for this operator would be the same as in the SM.

³This is not the case for single Higgs production for which $O_{\phi G}$ enters at $O(\alpha)$, while $O_{t\phi}$ and O_{tG} enter at $O(\alpha_s^2\alpha)$.

the relevant mixing terms are always $\mathcal{O}(\alpha_s)$. Had we chosen a different normalisation of operators, this would not be true.

We briefly discuss the mixing structure of these operators. The complete RG structure has been given in [75–77]. In this work we will consider the QCD induced mixing, which is relevant for our calculation, i.e. $\mathcal{O}(\alpha_s)$ terms with our normalisation. The mixing matrix for $(O_{t\phi}, O_{\phi G}, O_{tG})$ has a triangle form:

$$\frac{dC_i(\mu)}{d\log\mu} = \frac{\alpha_s}{\pi} \gamma_{ij} C_j(\mu), \quad \gamma = \begin{pmatrix} -2 & 16 & 8 \\ 0 & -7/2 & 1/2 \\ 0 & 0 & 1/3 \end{pmatrix}. \quad (2.5)$$

These operators involve three, two and one Higgs fields, respectively. In $t\bar{t}H$ production with only QCD corrections, only one of the Higgs fields can be dynamic, so in this sense their “dimensions” are 4, 5, 6 respectively. The triangle form of the matrix implies that only a “higher-dimensional” operator can mix into a “lower-dimensional one”, i.e. O_{tG} mixes into $O_{\phi G}$, and both of them mix into $O_{t\phi}$, but not the other way around.

Four-fermion operators that contribute to top-pair production would also play a role in this process. However the $t\bar{t}$ cross section measurement is sufficient to constrain this effect. There are four linear combinations of operators that enter, defined as $C_{u,d}^{1,2}$ in Ref. [90]. Using the notations of Ref. [91], they can be written as

$$C_u^1 = C_{qq}^{(1)1331} + C_{uu}^{1331} + C_{qq}^{(3)1331}, \quad (2.6)$$

$$C_u^2 = C_{qu}^{(8)1133} + C_{qu}^{(8)3311}, \quad (2.7)$$

$$C_d^1 = C_{qq}^{(3)1331} + \frac{1}{4} C_{ud}^{(8)3311}, \quad (2.8)$$

$$C_d^2 = C_{qu}^{(8)1133} + C_{qd}^{(8)3311}. \quad (2.9)$$

Consider $\sigma_{t\bar{t}}$ and $\sigma_{t\bar{t}H}$ at 8 TeV (at LO):

$$\sigma_{t\bar{t}}^{8TeV}[pb] = 158 [1 + 0.0101 (C_u^1 + C_u^2 + 0.64C_d^1 + 0.64C_d^2) + 0.65C_{tG}] \quad (2.10)$$

$$\sigma_{t\bar{t}H}^{8TeV}[pb] = 0.110 [1 + 0.055 (C_u^1 + C_u^2 + 0.61C_d^1 + 0.61C_d^2) + 2.02C_{tG}], \quad (2.11)$$

assuming $\Lambda = 1$ TeV. We can see that approximately only one linear combination of the four-fermion operator coefficients, i.e. $C_4 \simeq C_u^1 + C_u^2 + 0.6C_d^1 + 0.6C_d^2$ enters both cross sections, a pattern we do not expect to change at NLO. This behaviour is expected because the Higgs only couples to the top quark with the same coupling regardless of which operator triggers the process, so adding one Higgs does not resolve the degeneracy between four-fermion operators. It does, however, increase the relative sensitivity to these operators, because having a Higgs boson in the final state largely increases the center of mass energy of the process, which in turn increases the relative contribution from the four-fermion operators. On the other hand, the C_{tG} contribution is independent of C_4 , and this is because the Higgs particle can be emitted not only from the top quark but also from the operator O_{tG} with a four-point contact $gt\bar{t}H$ or a five-point $gg\bar{t}tH$ vertex, leading to a different topology than the four-fermion operator cases. Since we are going to focus on the $t\bar{t}H$ process, as

a first approximation we assume that the $t\bar{t}$ measurement is already constraining C_4 . A complete treatment at NLO including four-fermion operators requires a dedicated study which we defer to future work. Alternatively, one could make use of the ratio of the two cross sections:

$$\frac{\sigma_{t\bar{t}h}^{8TeV}}{\sigma_{t\bar{t}}^{8TeV}(\sqrt{\hat{s}} > 1000\text{GeV})} = 0.047[1 + 1.43C_{tG} + 0.0016(C_u^1 + C_u^2) + 0.0028(C_d^1 + C_d^2)], \quad (2.12)$$

which will decrease the dependence on the four-fermion operators by one order of magnitude. (A similar ratio has been proposed for $t\bar{t}Z$ [92].) In any case, the fact that four-fermion operators enter as one linear combination in $t\bar{t}$ and $t\bar{t}H$ will allow us to focus on O_{tG} , $O_{t\phi}$ and $O_{\phi G}$ in the $t\bar{t}H$ process. We should also mention that, by making use of Tevatron data and asymmetry measurements, all the relevant four-fermion operators can in principle be constrained from $t\bar{t}$ measurements [66–68, 93].

The final goal of top-quark measurements is to construct a global fit, where by combining $t\bar{t}$ and $t\bar{t}H$ processes we will be able to set bounds on C_4 and the other coefficients separately. Intuitively, however, it is useful to have an approximate understanding of which operators are constrained by which process. $t\bar{t}$ has often been thought of as the key process to bound O_{tG} , but what we are proposing here is to use $t\bar{t}$ to constrain four-fermion operators, while O_{tG} will be better constrained by $t\bar{t}H$ together with the other two operators, $O_{t\phi}$ and $O_{\phi G}$. As we will see in Section 7, even though this is not exactly the case with the current measurements, it is likely to happen in the future for high luminosity LHC (HL-LHC), because the $t\bar{t}H$ process is more sensitive to O_{tG} than the $t\bar{t}$ process, as can be seen from Eq. (2.11), and its measurement has more room to improve.

Finally, another operator that contributes to the processes is $O_G = g_s f^{ABC} G_\mu^{A\nu} G_\nu^{B\rho} G_\rho^{C\mu}$, which would enter by modifying the gluon self-interactions. As this is not a top-quark operator, we will not consider it further here, assuming also that its contribution is sufficiently suppressed due to constraints from the accurately measured $t\bar{t}$ and dijet cross sections.

3 Calculation setup

Our computation is performed within the MG5_AMC framework [78], as described in [43–45]. All the elements entering the NLO computations are available automatically starting from the SMEFT Lagrangian [94–99]. NLO results can be matched to parton shower programs, such as PYTHIA8 [100] and HERWIG++ [101], through the MC@NLO [102] formalism.

Special care needs to be taken for the UV counterterms, which are required for the virtual corrections. With \overline{MS} the coefficient renormalisation is

$$C_i^0 = Z_{ij}C_j, \quad \delta Z_{ij} = \frac{\alpha_s}{2\pi}\Delta(\mu_{EFT})\frac{1}{\epsilon}\gamma_{ij}, \quad (3.1)$$

where μ_{EFT} is the scale at which we define the EFT, and

$$\Delta(x) \equiv \Gamma(1 + \epsilon) \left(\frac{4\pi\mu^2}{x^2} \right)^\epsilon. \quad (3.2)$$

The $\Delta(\mu_{EFT})$ is inserted to separate the running of operator coefficients from the running of α_s . In other words, these coefficients are always defined at scale μ_{EFT} . They run and mix whenever μ_{EFT} changes.

The δZ_{ij} and fields/coupling renormalisations determine all the counterterms. However, in practice, we define the $O_{t\phi}$ and $O_{\phi G}$ operators as

$$\bar{O}_{t\phi} = y_t^3 \left(\phi^\dagger \phi - v^2/2 \right) (\bar{Q}t) \tilde{\phi} \quad (3.3)$$

$$\bar{O}_{\phi G} = y_t^2 \left(\phi^\dagger \phi - v^2/2 \right) G_{\mu\nu}^A G^{A\mu\nu}, \quad (3.4)$$

to remove the dimension-four terms due to Higgs fields taking vevs, so that there is no need to redefine the SM fields and masses etc.. In principle this does not change any physics; in practice the UV counterterms need to be treated slightly differently. For example, O_{tG} mixes into $O_{\phi G}$, meaning that at one loop O_{tG} needs the following counterterms to cancel the divergence

$$\frac{1}{4} \frac{\alpha_s}{\pi} \frac{1}{\epsilon} y_t^2 \left(\phi^\dagger \phi \right) G_{\mu\nu}^A G^{A\mu\nu} + h.c. = \frac{\alpha_s}{4\pi} \frac{1}{\epsilon} \left[\bar{O}_{\phi G} + m_t^2 G_{\mu\nu}^A G^{A\mu\nu} + h.c. \right]. \quad (3.5)$$

With our redefinition, $\delta Z_{\phi G, tG}$ will only produce the first counterterm. The second term is of dimension four, corresponding to a modification to the SM counterterms for the gluon field and g_s . These are, however, only the divergent part. Finite pieces need to be added, for the gluon fields to be renormalised on-shell and for g_s to be subtracted at the zero-momentum transfer:

$$\delta Z_2^{(g)} = \delta Z_{2, SM}^{(g)} - C_{tG} \frac{2\alpha_s m_t^2}{\pi \Lambda^2} \Delta(m_t) \frac{1}{\epsilon_{UV}}, \quad (3.6)$$

$$\delta Z_{g_s} = \delta Z_{g_s, SM} + C_{tG} \frac{\alpha_s m_t^2}{\pi \Lambda^2} \Delta(m_t) \frac{1}{\epsilon_{UV}}. \quad (3.7)$$

Similarly the top-quark field and top-Yukawa renormalisation are related to $O_{tG} \rightarrow O_{t\phi}$ mixing:

$$\delta Z_{m_t} = \delta Z_{y_t} = \delta Z_{m_t, SM} - C_{tG} \frac{4\alpha_s m_t^2}{\pi \Lambda^2} \Delta(m_t) \left(\frac{1}{\epsilon_{UV}} + \frac{1}{3} \right), \quad (3.8)$$

$$\delta Z_2^{(t)} = \delta Z_{2, SM}^{(t)} - C_{tG} \frac{2\alpha_s m_t^2}{\pi \Lambda^2} \Delta(m_t) \left(\frac{1}{\epsilon_{UV}} + \frac{1}{3} \right). \quad (3.9)$$

In summary, we calculate UV counterterms by using δZ_{ij} in Eq. (3.1) for O_{tG} , $\bar{O}_{\phi G}$, and $\bar{O}_{t\phi}$, while modifying the SM counterterms as described in Eqs. (3.6-3.9). In the following sections we will simply denote \bar{O} by O .

4 Theoretical uncertainties

One of the motivations to perform a NLO computation is that this provides the possibility to assess reliably the size of the residual uncertainties from missing higher orders. Discussions about the impact and the methods to estimate theoretical uncertainties in the SMEFT can

be found in Refs. [103–107]. Here, before moving on to numerical results, we briefly discuss how theoretical uncertainties are treated in our calculation.

The SMEFT calculation is an expansion in two classes of parameters, the perturbative expansion parameters, such as α_s and α , and the EFT expansion parameter C/Λ^2 , and so there are two main types of theoretical uncertainties, those related to missing higher orders in the gauge couplings and those from higher-order terms in the C/Λ^2 expansion. In the former class, we can list:

- Uncertainties due to parton-distribution functions.

This type of uncertainty is also present in the SM calculations and can be treated in the same way, i.e. by following the procedures associated with the corresponding PDF sets.

- Uncertainties due to missing higher orders in the α_s expansion as in the SM.

These are typically estimated by varying the renormalisation and factorisation scales, as in SM calculations. All results presented in this work are provided with uncertainties that are estimated by varying these two scales independently by a factor of two up and down from the central value. The uncertainties due to higher orders in α are expected to be subdominant.

- Uncertainties due to missing higher orders in the α_s expansion of the EFT operators.

These are additional uncertainties, related to the scale μ_{EFT} , at which the operators are defined. This uncertainty characterises the uncanceled logarithmic terms in the renormalisation group running and mixing of the operators. They can be obtained as follows: consider the cross section obtained at the central scale, $\mu_{EFT} = \mu_0$

$$\sigma(\mu_0) = \sigma_{SM} + \sum_i \frac{1\text{TeV}^2}{\Lambda^2} C_i(\mu_0) \sigma_i(\mu_0) + \sum_{i,j} \frac{1\text{TeV}^4}{\Lambda^4} C_i(\mu_0) C_j(\mu_0) \sigma_{ij}(\mu_0), \quad (4.1)$$

and at a different scale, $\mu_{EFT} = \mu$,

$$\sigma(\mu) = \sigma_{SM} + \sum_i \frac{1\text{TeV}^2}{\Lambda^2} C_i(\mu) \sigma_i(\mu) + \sum_{i,j} \frac{1\text{TeV}^4}{\Lambda^4} C_i(\mu) C_j(\mu) \sigma_{ij}(\mu) \quad (4.2)$$

$$= \sigma_{SM} + \sum_i \frac{1\text{TeV}^2}{\Lambda^2} C_i(\mu_0) \sigma_i(\mu_0; \mu) + \sum_{i,j} \frac{1\text{TeV}^4}{\Lambda^4} C_i(\mu_0) C_j(\mu_0) \sigma_{ij}(\mu_0; \mu), \quad (4.3)$$

where we define

$$\sigma_i(\mu_0; \mu) = \Gamma_{ji}(\mu, \mu_0) \sigma_j(\mu), \quad (4.4)$$

$$\sigma_{ij}(\mu_0; \mu) = \Gamma_{ki}(\mu, \mu_0) \Gamma_{lj}(\mu, \mu_0) \sigma_{kl}(\mu). \quad (4.5)$$

The Γ_{ij} describes the running of operator coefficients:

$$C_i(\mu) = \Gamma_{ij}(\mu, \mu_0) C_j(\mu_0), \quad (4.6)$$

and is given by

$$\Gamma_{ij}(\mu, \mu_0) = \exp \left(\frac{-2}{\beta_0} \log \frac{\alpha_s(\mu)}{\alpha_s(\mu_0)} \gamma_{ij} \right), \quad (4.7)$$

$$\beta_0 = 11 - 2/3n_f, \quad (4.8)$$

where $n_f = 5$ is the number of active flavors in the running of α_s .

According to Eq. (4.3), we will use $\sigma_{i,j}(\mu_0; \mu)$ with $\mu_0 = m_t$ and μ varying between $m_t/2$ and $2m_t$ to assess the EFT scale uncertainty. The physical interpretation is that they are the cross sections from $C(\mu_0)$, but evaluated at a different EFT scale μ , and then evolved back to scale μ_0 , with all the mixing and running effects taken into account, to allow for a fair comparison with the cross sections evaluated directly at μ_0 . A more detailed discussion of uncertainties specifically related to RG mixing effects with concrete examples will be presented in Section 6.

Now consider the uncertainties due to missing higher order contributions in the C/Λ^2 expansion. The cross section (or any other observable) can be written as:

$$\begin{aligned} \sigma = \sigma_{SM} &+ \sum_i \frac{C_i^{\text{dim6}}}{(\Lambda/1\text{TeV})^2} \sigma_i^{(\text{dim6})} + \sum_{i \leq j} \frac{C_i^{\text{dim6}} C_j^{\text{dim6}}}{(\Lambda/1\text{TeV})^4} \sigma_{ij}^{(\text{dim6})} \\ &+ \sum_i \frac{C_i^{\text{dim8}}}{(\Lambda/1\text{TeV})^4} \sigma_i^{(\text{dim8})} + \mathcal{O}(\Lambda^{-6}). \end{aligned} \quad (4.9)$$

The second term comes from the squared contribution of dimension-six operators, while the last term comes from the interference between the SM and dimension-eight operators. These two terms are formally $\mathcal{O}(\Lambda^{-4})$ contributions, but they should be considered separately [45, 106]. The last term must be less than the leading dimension-six contributions, otherwise the EFT expansion would break down and in that case one should not use the EFT approach from the very beginning. On the other hand, the second term can be much larger than the first one without invalidating the expansion, as can be justified for cases where the expansion in E^2/Λ^2 is under control but the squared contribution may still be large, due to less constrained operator coefficients, i.e. if $C_i^2 \frac{E^4}{\Lambda^4} > C_i \frac{E^2}{\Lambda^2} > 1 > \frac{E^2}{\Lambda^2}$ is satisfied. An example is given in [106]. Another possibility is that the interference term is suppressed due to symmetries, kinematics, or even simply accidentally [45], while the squared contribution is not. In the following we consider the two terms separately.

- Impact of the squared contributions $\sigma_{ij}^{(\text{dim6})}$ coming from dimension-six operators.

These terms can be explicitly calculated and included in the central prediction, and in that case there is no uncertainty related with this “expansion”, because there are no more terms beyond $(C/\Lambda^2)^2$. In this work we will give full results for $\sigma_{ij}^{(\text{dim6})}$. Of course, once constraints on operator coefficients are derived, one might decide to neglect some of these terms for simplicity. Only in this case should one use, for example $\sigma_{ii}^{(\text{dim6})}$, as an uncertainty estimate.

- Impact of missing higher-dimensional operators.

The contribution $\sigma_i^{(1,\text{dim}8)}$ cannot be computed without analysing dimension-eight operators. A corresponding uncertainty should be taken into account. For example, one can use s_{max}/Λ^2 to estimate the relative size of dimension-eight interference to dimension-six interference, where s_{max} is a cutoff on the centre-of-mass energy of the process, as applied in the analysis [106]. The results we present in this work are not computed with this cutoff, but with our setup this is straightforward.

5 Numerical results

In this section we give results for total cross sections and distributions. Results are obtained with MMHT2014 LO/NLO PDFs [108], for LO and NLO results respectively; input parameters are

$$m_t = 172.5 \text{ GeV}, \quad m_H = 125 \text{ GeV}, \quad m_Z = 91.1876 \text{ GeV}, \quad (5.1)$$

$$\alpha_{EW}^{-1} = 127.9, \quad G_F = 1.16637 \times 10^{-5} \text{ GeV}^{-2}. \quad (5.2)$$

Central scales for μ_R, μ_F are chosen as $m_t + m_H/2$ for the $t\bar{t}H$ process, and m_H for the other loop-induced processes. The central scale for μ_{EFT} is chosen as m_t for all processes.

5.1 Total cross sections

Cross sections from dimension-six operators can be parametrised as

$$\sigma = \sigma_{SM} + \sum_i \frac{1\text{TeV}^2}{\Lambda^2} C_i \sigma_i + \sum_{i \leq j} \frac{1\text{TeV}^4}{\Lambda^4} C_i C_j \sigma_{ij}. \quad (5.3)$$

Note that this parametrisation is slightly different from Eq. (4.1) because we have added a “ $i \leq j$ ” in the summation. In other words, for the cross terms (i.e. $\sigma_{ij}, i \neq j$), a factor of two from exchanging i, j will be included in σ_{ij} . We will now present results for σ_{SM} , σ_i , and σ_{ij} .

We quote numbers with three uncertainties. The first is the standard scale uncertainty, obtained by independently setting μ_R and μ_F to $\mu/2$, μ and 2μ , where μ is the central scale obtaining nine (μ_R, μ_F) combinations. The third uncertainty comes from the MMHT PDF sets. The second one is the EFT scale uncertainty, representing the missing higher-order corrections to the operators, obtained by using Eq. (4.3).

In Table 1 we give the LO/NLO results for $t\bar{t}H$ total cross section for the LHC at 8, 13 and 14 TeV. Both LO and NLO cross sections, as well as their ratios over the SM cross section, are given. In general the ratios to the SM contribution increase with energy, as expected in an EFT, except for the $O_{t\varphi}$ contributions which only rescale the SM Yukawa coupling. The quadratic terms and cross terms, i.e. σ_{ij} displayed in the last six rows, are in general not small, and we will see that given the current bounds on these operators they should not be neglected. The K factors range between roughly 1 to 1.6, depending on operators, and can be very different from the SM. In particular, contributions related to $O_{\varphi G}$ tend to have large K factors. Improved precision is clearly reflected by the reduced

8 TeV	σ LO	σ/σ_{SM} LO	σ NLO	σ/σ_{SM} NLO	K
σ_{SM}	$0.127^{+0.049+0.000+0.002}_{-0.032-0.000-0.001}$	$1.000^{+0.000+0.000+0.000}_{-0.000-0.000-0.000}$	$0.132^{+0.005+0.000+0.002}_{-0.012-0.000-0.002}$	$1.000^{+0.000+0.000+0.000}_{-0.000-0.000-0.000}$	1.03
$\sigma_{t\phi}$	$-0.015^{+0.004+0.001+0.000}_{-0.006-0.001-0.000}$	$-0.119^{+0.000+0.005+0.000}_{-0.000-0.006-0.000}$	$-0.016^{+0.002+0.000+0.000}_{-0.001-0.000-0.000}$	$-0.123^{+0.001+0.000+0.000}_{-0.002-0.002-0.000}$	1.07
$\sigma_{\phi G}$	$0.161^{+0.064+0.021+0.003}_{-0.042-0.017-0.002}$	$1.264^{+0.016+0.168+0.005}_{-0.015-0.137-0.003}$	$0.211^{+0.030+0.009+0.004}_{-0.030-0.007-0.004}$	$1.599^{+0.158+0.066+0.006}_{-0.091-0.052-0.009}$	1.31
σ_{tG}	$0.123^{+0.049+0.000+0.002}_{-0.032-0.000-0.001}$	$0.963^{+0.010+0.000+0.003}_{-0.009-0.002-0.002}$	$0.127^{+0.005+0.000+0.002}_{-0.012-0.001-0.002}$	$0.963^{+0.004+0.004+0.002}_{-0.003-0.007-0.003}$	1.03
$\sigma_{t\phi,t\phi}$	$0.0004^{+0.0002+0.0001+0.0000}_{-0.0001-0.0000-0.0000}$	$0.0035^{+0.0000+0.0004+0.0000}_{-0.0000-0.0002-0.0000}$	$0.0005^{+0.0000+0.0000+0.0000}_{-0.0001-0.0000-0.0000}$	$0.0036^{+0.0001+0.0002+0.0000}_{-0.0001-0.0000-0.0000}$	1.07
$\sigma_{\phi G,\phi G}$	$0.120^{+0.056+0.028+0.005}_{-0.035-0.021-0.003}$	$0.942^{+0.058+0.218+0.025}_{-0.048-0.161-0.014}$	$0.187^{+0.041+0.018+0.005}_{-0.035-0.015-0.006}$	$1.418^{+0.243+0.140+0.022}_{-0.148-0.115-0.028}$	1.56
$\sigma_{tG,tG}$	$0.118^{+0.056+0.002+0.005}_{-0.035-0.002-0.003}$	$0.929^{+0.060+0.015+0.026}_{-0.051-0.018-0.015}$	$0.126^{+0.007+0.001+0.004}_{-0.015-0.002-0.004}$	$0.959^{+0.017+0.008+0.015}_{-0.024-0.012-0.020}$	1.07
$\sigma_{t\phi,\phi G}$	$-0.010^{+0.003+0.001+0.000}_{-0.004-0.002-0.000}$	$-0.075^{+0.001+0.011+0.000}_{-0.001-0.014-0.000}$	$-0.013^{+0.002+0.001+0.000}_{-0.002-0.001-0.000}$	$-0.098^{+0.006+0.004+0.001}_{-0.011-0.007-0.000}$	1.34
$\sigma_{t\phi,tG}$	$-0.007^{+0.002+0.000+0.000}_{-0.003-0.000-0.000}$	$-0.058^{+0.001+0.003+0.000}_{-0.001-0.002-0.000}$	$-0.008^{+0.001+0.000+0.000}_{-0.000-0.000-0.000}$	$-0.060^{+0.001+0.001+0.000}_{-0.001-0.000-0.000}$	1.07
$\sigma_{\phi G,tG}$	$0.131^{+0.058+0.013+0.004}_{-0.037-0.011-0.002}$	$1.026^{+0.047+0.100+0.019}_{-0.040-0.083-0.011}$	$0.175^{+0.027+0.005+0.004}_{-0.028-0.004-0.005}$	$1.328^{+0.148+0.034+0.016}_{-0.095-0.031-0.021}$	1.34
13 TeV	σ LO	σ/σ_{SM} LO	σ NLO	σ/σ_{SM} NLO	K
σ_{SM}	$0.464^{+0.161+0.000+0.005}_{-0.111-0.000-0.004}$	$1.000^{+0.000+0.000+0.000}_{-0.000-0.000-0.000}$	$0.507^{+0.030+0.000+0.007}_{-0.048-0.000-0.008}$	$1.000^{+0.000+0.000+0.000}_{-0.000-0.000-0.000}$	1.09
$\sigma_{t\phi}$	$-0.055^{+0.013+0.002+0.000}_{-0.019-0.003-0.001}$	$-0.119^{+0.000+0.005+0.000}_{-0.000-0.006-0.000}$	$-0.062^{+0.006+0.001+0.001}_{-0.004-0.001-0.001}$	$-0.123^{+0.001+0.001+0.000}_{-0.001-0.002-0.000}$	1.13
$\sigma_{\phi G}$	$0.627^{+0.225+0.081+0.007}_{-0.153-0.067-0.005}$	$1.351^{+0.011+0.175+0.002}_{-0.011-0.145-0.001}$	$0.872^{+0.131+0.037+0.013}_{-0.123-0.035-0.016}$	$1.722^{+0.146+0.073+0.004}_{-0.089-0.068-0.005}$	1.39
σ_{tG}	$0.470^{+0.167+0.000+0.005}_{-0.114-0.002-0.004}$	$1.014^{+0.006+0.000+0.001}_{-0.006-0.004-0.001}$	$0.503^{+0.025+0.001+0.007}_{-0.046-0.003-0.008}$	$0.991^{+0.004+0.003+0.000}_{-0.010-0.006-0.001}$	1.07
$\sigma_{t\phi,t\phi}$	$0.0016^{+0.0005+0.0002+0.0000}_{-0.0004-0.0001-0.0000}$	$0.0035^{+0.0000+0.0004+0.0000}_{-0.0000-0.0003-0.0000}$	$0.0019^{+0.0001+0.0001+0.0000}_{-0.0002-0.0000-0.0000}$	$0.0037^{+0.0001+0.0002+0.0000}_{-0.0000-0.0001-0.0000}$	1.17
$\sigma_{\phi G,\phi G}$	$0.646^{+0.274+0.141+0.018}_{-0.178-0.107-0.010}$	$1.392^{+0.079+0.304+0.025}_{-0.066-0.231-0.014}$	$1.021^{+0.204+0.096+0.024}_{-0.178-0.085-0.029}$	$2.016^{+0.267+0.190+0.021}_{-0.178-0.167-0.027}$	1.58
$\sigma_{tG,tG}$	$0.645^{+0.276+0.011+0.020}_{-0.178-0.015-0.010}$	$1.390^{+0.082+0.023+0.028}_{-0.069-0.031-0.016}$	$0.674^{+0.036+0.004+0.016}_{-0.067-0.007-0.019}$	$1.328^{+0.011+0.008+0.014}_{-0.038-0.014-0.018}$	1.04
$\sigma_{t\phi,\phi G}$	$-0.037^{+0.009+0.006+0.000}_{-0.013-0.007-0.000}$	$-0.081^{+0.001+0.012+0.000}_{-0.001-0.015-0.000}$	$-0.053^{+0.008+0.003+0.001}_{-0.008-0.004-0.001}$	$-0.105^{+0.006+0.006+0.000}_{-0.009-0.007-0.000}$	1.42
$\sigma_{t\phi,tG}$	$-0.028^{+0.007+0.001+0.000}_{-0.010-0.001-0.000}$	$-0.060^{+0.000+0.002+0.000}_{-0.000-0.003-0.000}$	$-0.031^{+0.003+0.000+0.000}_{-0.002-0.000-0.000}$	$-0.061^{+0.000+0.000+0.000}_{-0.000-0.001-0.000}$	1.10
$\sigma_{\phi G,tG}$	$0.627^{+0.252+0.053+0.014}_{-0.166-0.047-0.008}$	$1.349^{+0.054+0.114+0.016}_{-0.046-0.100-0.009}$	$0.859^{+0.127+0.021+0.017}_{-0.126-0.020-0.022}$	$1.691^{+0.137+0.042+0.013}_{-0.097-0.039-0.017}$	1.37
14 TeV	σ LO	σ/σ_{SM} LO	σ NLO	σ/σ_{SM} NLO	K
σ_{SM}	$0.558^{+0.191+0.000+0.005}_{-0.132-0.000-0.004}$	$1.000^{+0.000+0.000+0.000}_{-0.000-0.000-0.000}$	$0.614^{+0.039+0.000+0.008}_{-0.058-0.000-0.009}$	$1.000^{+0.000+0.000+0.000}_{-0.000-0.000-0.000}$	1.10
$\sigma_{t\phi}$	$-0.066^{+0.016+0.003+0.001}_{-0.023-0.004-0.001}$	$-0.119^{+0.000+0.005+0.000}_{-0.000-0.007-0.000}$	$-0.075^{+0.008+0.001+0.001}_{-0.006-0.001-0.001}$	$-0.123^{+0.001+0.001+0.000}_{-0.001-0.002-0.000}$	1.14
$\sigma_{\phi G}$	$0.758^{+0.268+0.098+0.008}_{-0.184-0.081-0.006}$	$1.359^{+0.011+0.176+0.002}_{-0.010-0.144-0.001}$	$1.064^{+0.160+0.045+0.015}_{-0.149-0.040-0.018}$	$1.731^{+0.143+0.073+0.003}_{-0.087-0.066-0.004}$	1.40
σ_{tG}	$0.567^{+0.198+0.000+0.006}_{-0.136-0.001-0.005}$	$1.017^{+0.006+0.001+0.001}_{-0.005-0.001-0.001}$	$0.609^{+0.029+0.003+0.008}_{-0.054-0.002-0.009}$	$0.992^{+0.006+0.006+0.000}_{-0.014-0.003-0.000}$	1.07
$\sigma_{t\phi,t\phi}$	$0.0020^{+0.0007+0.0002+0.0000}_{-0.0005-0.0001-0.0000}$	$0.0036^{+0.0000+0.0003+0.0000}_{-0.0000-0.0002-0.0000}$	$0.0022^{+0.0002+0.0003+0.0000}_{-0.0002-0.0000-0.0000}$	$0.0036^{+0.0000+0.0005+0.0000}_{-0.0000-0.0000-0.0000}$	1.12
$\sigma_{\phi G,\phi G}$	$0.817^{+0.342+0.179+0.022}_{-0.223-0.134-0.012}$	$1.465^{+0.083+0.320+0.025}_{-0.069-0.240-0.014}$	$1.293^{+0.256+0.122+0.029}_{-0.223-0.105-0.036}$	$2.105^{+0.268+0.198+0.021}_{-0.182-0.170-0.027}$	1.58
$\sigma_{tG,tG}$	$0.819^{+0.345+0.014+0.024}_{-0.224-0.017-0.012}$	$1.468^{+0.087+0.025+0.028}_{-0.073-0.030-0.016}$	$0.852^{+0.046+0.007+0.019}_{-0.081-0.005-0.024}$	$1.388^{+0.014+0.011+0.014}_{-0.048-0.008-0.018}$	1.04
$\sigma_{t\phi,\phi G}$	$-0.045^{+0.011+0.006+0.000}_{-0.016-0.009-0.000}$	$-0.081^{+0.001+0.012+0.000}_{-0.001-0.016-0.000}$	$-0.065^{+0.009+0.004+0.001}_{-0.010-0.005-0.001}$	$-0.105^{+0.006+0.006+0.000}_{-0.009-0.008-0.000}$	1.44
$\sigma_{t\phi,tG}$	$-0.033^{+0.008+0.001+0.000}_{-0.012-0.002-0.000}$	$-0.060^{+0.000+0.002+0.000}_{-0.000-0.003-0.000}$	$-0.038^{+0.004+0.001+0.001}_{-0.002-0.000-0.000}$	$-0.062^{+0.000+0.001+0.000}_{-0.001-0.000-0.000}$	1.13
$\sigma_{\phi G,tG}$	$0.783^{+0.310+0.066+0.016}_{-0.205-0.056-0.009}$	$1.403^{+0.056+0.119+0.016}_{-0.048-0.101-0.009}$	$1.070^{+0.154+0.033+0.021}_{-0.154-0.024-0.026}$	$1.741^{+0.132+0.053+0.012}_{-0.096-0.039-0.016}$	1.37

Table 1. Total cross section in pb for $pp \rightarrow t\bar{t}H$ at 8, 13, and 14 TeV, as parametrised in Eq. (5.3).

uncertainties at NLO. The dominant uncertainties come from $\mu_{R,F}$ scale variation. However, these uncertainties, together with the PDF uncertainties, are reduced once taking ratios with respect to σ_{SM} . On the contrary, the EFT scale uncertainty is not affected by taking ratios, so it becomes relatively more important. This means that in a measurement where ratios are used, for example as proposed by [10], or in a global fit where correlations are correctly taken into account, the EFT uncertainties may be the dominant ones at dimension-six. We also note here that at the NLO accuracy the effect of the $O_{t\varphi}$ operator is not a simple rescaling of the SM prediction, because the y_t in the SM is defined with on-shell

8 TeV	σ LO	σ/σ_{SM} LO
σ_{SM}	$8.08^{+2.11+0.000}_{-1.60-0.000}$	$1.000^{+0.000+0.000}_{-0.000-0.000}$
$\sigma_{t\phi}$	$-0.962^{+0.190+0.043}_{-0.252-0.049}$	$-0.119^{+0.000035+0.0053}_{-0.000039-0.0061}$
$\sigma_{\phi G}$	$551.0^{+71.1+50.8}_{-62.8-42.6}$	$68.2^{+7.70+6.29}_{-7.64-5.27}$
σ_{tG}	$5.47^{+1.43+0.657}_{-1.08-1.88}$	$0.677^{+0.000029+0.081}_{-0.000059-0.23}$
$\sigma_{t\phi,t\phi}$	$0.0286^{+0.0075+0.00301}_{-0.0057-0.00250}$	$0.00354^{+0.000000+0.00037}_{-0.000001-0.00031}$
$\sigma_{\phi G,\phi G}$	$9289^{+24.2+1792}_{-130-1382}$	$1149^{+263+222}_{-236-171}$
$\sigma_{tG,tG}$	$0.924^{+0.2415+5.44}_{-0.1826-0.0}$	$0.1144^{+0.000000+0.673}_{-0.000002-0.0}$
$\sigma_{t\phi,\phi G}$	$-32.57^{+3.673+3.86}_{-4.146-4.83}$	$-4.030^{+0.447+0.478}_{-0.449-0.597}$
$\sigma_{t\phi,tG}$	$-0.326^{+0.0643+0.125}_{-0.0851-0.0407}$	$-0.0403^{+0.000005+0.0154}_{-0.000003-0.0050}$
$\sigma_{\phi G,tG}$	$185.08^{+22.96+0.0}_{-20.38-393}$	$22.90^{+2.495+0.0}_{-2.491-48.7}$
13 TeV	σ LO	σ/σ_{SM} LO
σ_{SM}	$19.6^{+5.47+0.000}_{-4.17-0.000}$	$1.000^{+0.000+0.000}_{-0.000-0.000}$
$\sigma_{t\phi}$	$-2.34^{+0.439+0.104}_{-0.576-2.46}$	$-0.119^{+0.000004+0.0053}_{-0.000006-0.0061}$
$\sigma_{\phi G}$	$1307^{+183.9+120}_{-166.0-101}$	$66.7^{+7.29+6.16}_{-7.24-5.16}$
σ_{tG}	$13.28^{+3.71+1.99}_{-2.83-4.90}$	$0.678^{+0.000051+0.102}_{-0.000018-0.250}$
$\sigma_{t\phi,t\phi}$	$0.0695^{+0.0194+0.00732}_{-0.0148-0.00607}$	$0.00355^{+0.0000+0.00037}_{-0.0000-0.00031}$
$\sigma_{\phi G,\phi G}$	$22515^{+377+4340}_{-732-3350}$	$1150^{+264+222}_{-236-171}$
$\sigma_{tG,tG}$	$2.253^{+0.631+13.2}_{-0.481-0.0}$	$0.115^{+0.000050+0.676}_{-0.000062-0.0}$
$\sigma_{t\phi,\phi G}$	$-76.8^{+9.38+9.11}_{-10.3-11.4}$	$-3.923^{+0.446+0.47}_{-0.453-0.58}$
$\sigma_{t\phi,tG}$	$-0.799^{+0.171+0.332}_{-0.224-0.134}$	$-0.04078^{+0.000062+0.017}_{-0.000050-0.007}$
$\sigma_{\phi G,tG}$	$450^{+63.3+0.0}_{-57.3-954}$	$23.0^{+2.50+0.0}_{-2.49-48.7}$
14 TeV	σ LO	σ/σ_{SM} LO
σ_{SM}	$22.4^{+6.41+0.000}_{-4.87-0.000}$	$1.000^{+0.000+0.000}_{-0.000-0.000}$
$\sigma_{t\phi}$	$-2.66^{+0.576+0.118}_{-0.757-0.136}$	$-0.118^{+0.000065+0.00529}_{-0.000080-0.00608}$
$\sigma_{\phi G}$	$1509^{+224+139}_{-203-117}$	$67.3^{+7.47+6.20}_{-7.50-5.20}$
σ_{tG}	$15.1^{+4.296+2.06}_{-3.27-5.33}$	$0.673^{+0.000628+0.092}_{-0.000506-0.238}$
$\sigma_{t\phi,t\phi}$	$0.0791^{+0.0225+0.00832}_{-0.0171-0.0069}$	$0.00352^{+0.000003+0.00037}_{-0.000002-0.00031}$
$\sigma_{\phi G,\phi G}$	$2564^{+546+4947}_{-962-3813}$	$1143^{+263+221}_{-235-170}$
$\sigma_{tG,tG}$	$2.55^{+0.727+15.1}_{-0.553-0.0}$	$0.114^{+0.000074+0.673}_{-0.000060-0.0}$
$\sigma_{t\phi,\phi G}$	$-89.5^{+12.85+10.6}_{-14.1-13.2}$	$-3.99^{+0.479+0.473}_{-0.478-0.59}$
$\sigma_{t\phi,tG}$	$-0.895^{+0.194+0.340}_{-0.254-0.204}$	$-0.0399^{+0.000046+0.0152}_{-0.000057-0.0091}$
$\sigma_{\phi G,tG}$	$515^{+75.2+0.0}_{-67.8-1089}$	$22.94^{+2.506+0.0}_{-2.490-48.6}$

Table 2. Total cross section in pb for $pp \rightarrow H$ at 8, 13, and 14 TeV, as parametrised in Eq. (5.3). Only the renormalisation and factorisation and EFT scale uncertainties are shown.

top mass, while the $C_{t\varphi}$ is defined with the \overline{MS} scheme. As a result the corresponding K factors are different from the SM ones.

The corresponding LO results for single H production are shown in Table 2, where we have kept the exact top mass dependence. The PDF uncertainties are not shown as these are found to be at the percent level and significantly smaller than the $\mu_{R,F}$ scale uncertainties. We note that these results suffer from large $\mu_{R,F}$ scale uncertainties as they are at LO. As in the case of $t\bar{t}H$ we find that the $\mu_{R,F}$ scale uncertainties get significantly reduced by taking the ratio over the SM. This reduction of the uncertainties in the ratios is not dramatic for

8 TeV	σ NLO	σ/σ_{SM} NLO
σ_{SM}	$13.54^{+2.812}_{-2.192}$	$1.000^{+0.000}_{-0.000}$
$\sigma_{t\phi}$	$-1.577^{+0.252}_{-0.322}$	$-0.117^{+0.000369}_{-0.000305}$
$\sigma_{\phi G}$	1036^{+140}_{-113}	$76.5^{+4.797}_{-4.632}$
$\sigma_{t\phi,t\phi}$	$0.0459^{+0.0092}_{-0.0072}$	$0.00339^{+0.000018}_{-0.000022}$
$\sigma_{\phi G,\phi G}$	19802^{+1319}_{-1120}	1463^{+184}_{-171}
13 TeV	σ NLO	σ/σ_{SM} NLO
σ_{SM}	$31.29^{+7.08}_{-5.68}$	$1.000^{+0.000}_{-0.000}$
$\sigma_{t\phi}$	$-3.646^{+0.653}_{-0.809}$	$-0.117^{+0.000416}_{-0.000339}$
$\sigma_{\phi G}$	2395^{+365}_{-309}	$76.5^{+4.89}_{-4.67}$
$\sigma_{t\phi,t\phi}$	$0.106^{+0.0231}_{-0.0187}$	$0.00339^{+0.000020}_{-0.000025}$
$\sigma_{\phi G,\phi G}$	45785^{+3817}_{-3493}	1463^{+188}_{-173}
14 TeV	σ NLO	σ/σ_{SM} NLO
σ_{SM}	$35.33^{+8.07}_{-6.50}$	$1.000^{+0.000}_{-0.000}$
$\sigma_{t\phi}$	$-4.117^{+0.747}_{-0.922}$	$-0.117^{+0.000425}_{-0.000344}$
$\sigma_{\phi G}$	2704^{+418}_{-356}	$76.5^{+4.91}_{-4.68}$
$\sigma_{t\phi,t\phi}$	$0.120^{+0.0263}_{-0.0215}$	$0.00339^{+0.000020}_{-0.000025}$
$\sigma_{\phi G,\phi G}$	51700^{+4410}_{-4070}	1463^{+189}_{-173}

Table 3. Total cross section in pb for $pp \rightarrow H$ at 8, 13, and 14 TeV at NLO in the infinite top mass limit. Only the renormalisation and factorisation scale uncertainties are shown.

the $O_{\phi G}$ contributions. This is related to the choice of operator normalisation, which leads to $O_{\phi G}$ entering at $O(\alpha)$ while the SM contribution is at $O(\alpha_s^2\alpha)$. We also find that the ratios over the SM are not sensitive to the collider energy as the partonic centre-of-mass energy is fixed at the Higgs mass. Again we find that σ_{ij} terms are important. For this process, we find that the contributions involving the $O_{\phi G}$ operator are large as it enters at tree-level while the other two operators enter through top-quark loops.

While the computation of the NLO corrections for the $O_{t\phi}$ and $O_{\phi G}$ operators is possible both in the infinite top mass limit and with the exact top-mass dependence, this is not the case for the O_{tG} operator for which a dedicated computation, beyond the scope of this work, is required. As a first step towards NLO results, we show in Table 3 results for a subset of the contributions computed in the infinite top mass limit. The results show the well-known large K factors (~ 2) for gluon fusion and demonstrate the reduction of the $\mu_{R,F}$ uncertainties.

The results for the $pp \rightarrow Hj$ process are shown in Table 4. For these results a 30 GeV cut has been imposed on the jet transverse momentum. The relative contributions of the operators at the total cross-section level remain similar to those for single H as the cut on the jet is rather soft. While $O_{t\phi}$ just gives a rescaling compared to the SM, the $O_{\phi G}$ and O_{tG} operators have a different energy dependence causing also small differences in the ratios between the three collider energies, as a range of partonic energies is probed.

Finally we show the results for Higgs pair production in Table 5. This process behaves in a different way than the single Higgs production process. The contribution of $O_{t\phi}$ operator is no longer a simple universal rescaling of the SM, as it not only affects the triangle, box

8 TeV	σ LO	σ/σ_{SM} LO
σ_{SM}	$4.168^{+2.05+0.000}_{-1.28-0.000}$	$1.000^{+0.000+0.000}_{-0.000-0.000}$
$\sigma_{t\phi}$	$-0.495^{+0.152+0.022}_{-0.244-0.025}$	$-0.119^{+0.000027+0.0053}_{-0.000045-0.0061}$
$\sigma_{\phi G}$	$270.6^{+86.1+25.0}_{-61.0-20.9}$	$64.9^{+7.62+5.99}_{-7.55-5.02}$
σ_{tG}	$2.85^{+1.40+0.549}_{-0.874-1.13}$	$0.683^{+0.000212+0.132}_{-0.000071-0.271}$
$\sigma_{t\phi,t\phi}$	$0.0147^{+0.0072+0.00154}_{-0.0045-0.00128}$	$0.00352^{+0.000001+0.00037}_{-0.000001-0.00031}$
$\sigma_{\phi G,\phi G}$	$4875^{+909+940}_{-725-724}$	$1170^{+269+226}_{-241-173}$
$\sigma_{tG,tG}$	$0.496^{+0.246+0.214}_{-0.153-0.318}$	$0.119^{+0.000276+0.051}_{-0.000206-0.076}$
$\sigma_{t\phi,\phi G}$	$-16.5^{+3.82+1.96}_{-5.42-2.45}$	$-3.97^{+0.43+0.47}_{-0.43-0.59}$
$\sigma_{t\phi,tG}$	$-0.167^{+0.051+0.064}_{-0.082-0.047}$	$-0.0400^{+0.000031+0.0154}_{-0.000045-0.011}$
$\sigma_{\phi G,tG}$	$100.8^{+33.4+15.0}_{-23.4-44.5}$	$24.17^{+2.63+3.59}_{-2.61-10.7}$
13 TeV	σ LO	σ/σ_{SM} LO
σ_{SM}	$11.49^{+5.091+0.000}_{-3.296-0.000}$	$1.000^{+0.000+0.000}_{-0.000-0.000}$
$\sigma_{t\phi}$	$-1.378^{+0.393+0.0615}_{-0.604-0.0707}$	$-0.1200^{+0.000379+0.00535}_{-0.000321-0.0061}$
$\sigma_{\phi G}$	$792^{+220.4+73.0}_{-163-61.2}$	$68.9^{+7.89+6.36}_{-7.89-5.33}$
σ_{tG}	$7.91^{+3.50+0.984}_{-2.27-2.71}$	$0.689^{+0.000223+0.0857}_{-0.000253-0.235}$
$\sigma_{t\phi,t\phi}$	$0.0410^{+0.0180+0.0043}_{-0.0117-0.0036}$	$0.003574^{+0.000008+0.00038}_{-0.000010-0.00031}$
$\sigma_{\phi G,\phi G}$	$13663^{+2021+2636}_{-1697-2032}$	$1189^{+274+229}_{-245-177}$
$\sigma_{tG,tG}$	$1.400^{+0.625+0.454}_{-0.404-0.890}$	$0.122^{+0.000257+0.0395}_{-0.000193-0.0774}$
$\sigma_{t\phi,\phi G}$	$-46.5^{+9.62+5.51}_{-13.1-6.89}$	$-4.04^{+0.454+0.48}_{-0.453-0.60}$
$\sigma_{t\phi,tG}$	$-0.470^{+0.134+0.180}_{-0.207-0.084}$	$-0.0409^{+0.000079+0.0157}_{-0.000068-0.0073}$
$\sigma_{\phi G,tG}$	$282^{+85.2+50.4}_{-61.3-124}$	$24.6^{+3.02+4.39}_{-2.91-10.8}$
14 TeV	σ LO	σ/σ_{SM} LO
σ_{SM}	$13.35^{+5.79+0.000}_{-3.78-0.000}$	$1.000^{+0.000+0.000}_{-0.000-0.000}$
$\sigma_{t\phi}$	$-1.589^{+0.451+0.0709}_{-0.693-0.0815}$	$-0.1190^{+0.000132+0.0053}_{-0.000159-0.0061}$
$\sigma_{\phi G}$	$905^{+254+83.4}_{-186-70.0}$	$67.74^{+7.567+6.25}_{-7.483-5.24}$
σ_{tG}	$9.223^{+4.03+1.38}_{-2.62-3.33}$	$0.691^{+0.001289+0.103}_{-0.001025-0.25}$
$\sigma_{t\phi,t\phi}$	$0.0472^{+0.0205+0.00497}_{-0.0134-0.00412}$	$0.00354^{+0.000000+0.00037}_{-0.000000-0.00031}$
$\sigma_{\phi G,\phi G}$	$15820^{+2254+3050}_{-1907-2350}$	$1185^{+275+229}_{-245-176}$
$\sigma_{tG,tG}$	$1.631^{+0.7185+0.87}_{-0.4660.49}$	$0.122^{+0.000567+0.037}_{-0.000437-0.065}$
$\sigma_{t\phi,\phi G}$	$-54.8^{+11.3+6.49}_{-15.3-8.12}$	$-4.10^{+0.45+0.486}_{-0.45-0.608}$
$\sigma_{t\phi,tG}$	$-0.554^{+0.158+0.208}_{-0.244-0.076}$	$-0.0414^{+0.000156+0.0156}_{-0.000199-0.0057}$
$\sigma_{\phi G,tG}$	$323^{+91.3+65.9}_{-67.4-125}$	$24.19^{+2.63+4.93}_{-2.65-9.38}$

Table 4. Total cross section in pb for $pp \rightarrow Hj$ at 8, 13, and 14 TeV at LO for a $p_T^j > 30$ GeV cut. Only the $\mu_{R,F}$ and EFT scale uncertainties are shown.

diagrams and their interference in a different way but also introduces the $ttHH$ interaction. Thus the ratio over the SM behaves differently from single Higgs production and also acquires an energy dependence. The contributions involving $O_{\phi G}$ and O_{tG} relative to the SM increase with the collider energy. The EFT scale uncertainties in the ratios over the SM are similar in size to the $\mu_{R,F}$ ones for $O_{\phi G}$, while they dominate for O_{tG} and $O_{t\phi}$. We find that the contribution of the chromo-dipole is large, and even with the current constraints it could have a large impact on HH production. This observation implies that an EFT analysis of di-Higgs production should consistently take into consideration such

8 TeV	σ LO	σ/σ_{SM} LO
σ_{SM}	$0.00755^{+0.00313+0.000}_{-0.00206-0.000}$	$1.000^{+0.000+0.000}_{-0.000-0.000}$
$\sigma_{t\phi}$	$0.00167^{+0.000704+0.000086}_{-0.000459-0.000075}$	$0.221^{+0.00111+0.0113}_{-0.000876-0.0099}$
$\sigma_{\phi G}$	$-0.348^{+0.0676+0.0273}_{-0.0903-0.0325}$	$-46.0^{+5.04+3.61}_{-4.93-4.31}$
σ_{tG}	$-0.0111^{+0.00290+0.00183}_{-0.00432-0.0010}$	$-1.46^{+0.0244+0.243}_{-0.0203-0.135}$
$\sigma_{t\phi,t\phi}$	$0.000198^{+0.000088+0.0000208}_{0.000057-0.0000173}$	$0.0262^{+0.00060+0.0028}_{-0.00048-0.0023}$
$\sigma_{\phi G,\phi G}$	$19.42^{+2.67+3.75}_{-2.19-2.89}$	$2571^{+626+497}_{-544-383}$
$\sigma_{tG,tG}$	$0.0127^{+0.00559+0.00133}_{-0.00359-0.00323}$	$1.69^{+0.0289+0.176}_{-0.0209-0.427}$
$\sigma_{t\phi,\phi G}$	$-0.0853^{+0.0186+0.010}_{-0.0257-0.013}$	$-11.29^{+1.54+1.35}_{-1.62-1.69}$
$\sigma_{t\phi,tG}$	$-0.00255^{+0.000700+0.000546}_{0.00107-0.000323}$	$-0.337^{+0.00113+0.072}_{-0.00127-0.043}$
$\sigma_{\phi G,tG}$	$0.987^{+0.277+0.143}_{-0.199-0.202}$	$130.7^{+16.4+18.9}_{-15.4-26.8}$
13 TeV	σ LO	σ/σ_{SM} LO
σ_{SM}	$0.0256^{+0.00904+0.000}_{-0.00625-0.000}$	$1.000^{+0.000+0.000}_{-0.000-0.000}$
$\sigma_{t\phi}$	$0.00580^{+0.00209+0.000297}_{-0.00144-0.000259}$	$0.227^{+0.00114+0.0116}_{-0.000918-0.0101}$
$\sigma_{\phi G}$	$-1.208^{+0.231+0.0948}_{-0.291-0.113}$	$-47.3^{+6.18+3.707}_{-6.14-4.42}$
σ_{tG}	$-0.0347^{+0.00804+0.0041}_{-0.0113-0.0013}$	$-1.356^{+0.0271+0.161}_{-0.0225-0.051}$
$\sigma_{t\phi,t\phi}$	$0.000748^{+0.000290+0.000079}_{-0.000194-0.000065}$	$0.0293^{+0.000727+0.0031}_{-0.000584-0.0026}$
$\sigma_{\phi G,\phi G}$	$73.02^{+7.54+14.1}_{-6.48-10.9}$	$2856.2^{+743.3+552}_{-628.5-425}$
$\sigma_{tG,tG}$	$0.0496^{+0.0198+0.00505}_{-0.01305-0.0126}$	$1.940^{+0.0650+0.198}_{-0.0477-0.493}$
$\sigma_{t\phi,\phi G}$	$-0.303^{+0.0506+0.0362}_{-0.0641-0.0453}$	$-11.83^{+1.39+1.42}_{-1.41-1.77}$
$\sigma_{t\phi,tG}$	$-0.00870^{+0.00213+0.00163}_{-0.00309-0.00120}$	$-0.340^{+0.000238+0.064}_{-0.000438-0.047}$
$\sigma_{\phi G,tG}$	$3.77^{+0.914+0.554}_{-0.681-0.802}$	$147.5^{+20.83+20.7}_{-18.86-31.4}$
14 TeV	σ LO	σ/σ_{SM} LO
σ_{SM}	$0.0305^{+0.0105+0.000}_{-0.00734-0.000}$	$1.000^{+0.000+0.000}_{-0.000-0.000}$
$\sigma_{t\phi}$	$0.00694^{+0.00245+0.00031}_{-0.00169-0.00036}$	$0.227^{+0.00131+0.0117}_{-0.00106-0.0101}$
$\sigma_{\phi G}$	$-1.508^{+0.214+0.118}_{-0.256-0.141}$	$-49.4^{+6.45+3.87}_{-6.39-4.61}$
σ_{tG}	$-0.0408^{+0.00929+0.0037}_{-0.0130-0.0008}$	$-1.337^{+0.0271+0.122}_{-0.0224-0.0262}$
$\sigma_{t\phi,t\phi}$	$0.000904^{+0.000343+0.000095}_{-0.000232-0.000079}$	$0.0296^{+0.00076+0.0031}_{-0.00061-0.0026}$
$\sigma_{\phi G,\phi G}$	$88.35^{+8.72+17.1}_{-7.55-13.2}$	$2896^{+741+560}_{-641-431}$
$\sigma_{tG,tG}$	$0.0608^{+0.0241+0.00605}_{-0.0159-0.0148}$	$1.994^{+0.0753+0.198}_{-0.0556-0.484}$
$\sigma_{t\phi,\phi G}$	$-0.367^{+0.0520+0.0439}_{-0.0670-0.0550}$	$-12.0^{+1.46+1.44}_{-1.56-1.80}$
$\sigma_{t\phi,tG}$	$-0.0104^{+0.00253+0.00192}_{-0.00368-0.00174}$	$-0.341^{+0.0014+0.063}_{-0.002-0.057}$
$\sigma_{\phi G,tG}$	$4.60^{+1.09+0.640}_{-0.816-0.923}$	$150.7^{+21.69+21.0}_{-19.53-30.3}$

Table 5. Total cross section in pb for $pp \rightarrow HH$ at 8, 13, and 14 TeV at LO. Only the $\mu_{R,F}$ and EFT scale uncertainties are shown.

an impact, as it will affect the limits set on other dimension-six operators entering the process, in particular those modifying the Higgs self-coupling. We also emphasize that this contribution involves a UV pole that is canceled by the mixing from O_{tG} to $O_{\phi G}$, therefore its cross section has a dependence on μ_{EFT} , and should always be used with care. The EFT uncertainty presented in Table 5 correctly takes into account the contribution from $O_{\phi G}$ through mixing effects while changing μ_{EFT} . A more detailed discussion on this issue will be presented in Section 6.

5.2 Distributions

Differential distributions are obtained at LO and NLO for the $pp \rightarrow t\bar{t}H$ process. This can be done also with matching to PS simulation, and with top quarks decayed while keeping spin correlations [109], all implemented in the MG5_AMC framework. Hence our approach can be used directly in a realistic experimental simulation, with NLO+PS event generation, which allows for more detailed studies of possible EFT signals. In this work, for illustration purpose, we only present fixed order NLO distributions.

Results for $t\bar{t}H$ are given in Figures 3-6. The SM contribution as well as the individual operator contributions, normalised, are displayed, in order to compare the kinematic features from different operators. The magnitudes can be read off from the total cross section tables. In the lower panel we give the differential K factors for each operator, together with the $\mu_{R,F}$ uncertainties. Both interference and squared contributions are shown.

The interference contributions are in general not sensitive to the operator, except for a few cases such as $m(tH)$ and $p_T(H)$, which should be considered as discriminating observables in a differential measurement. On the contrary, the squared contributions can be quite sensitive, and many of them can be used to distinguish between the contributions from $O_{\varphi G}$, O_{tG} , and those from SM background and $O_{t\varphi}$. Given the current limits on the coefficients, it is likely that the O_{tG} operator still leads to observable effects on the shape, due to large squared contributions. As an example we plot some total distributions for

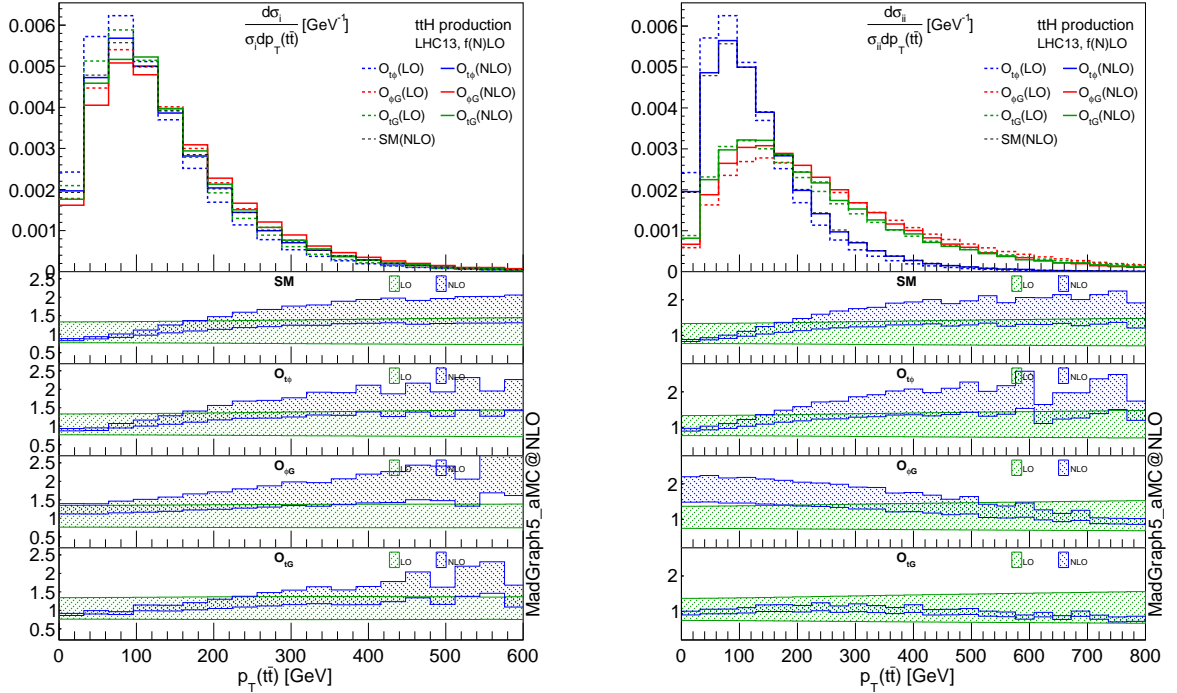


Figure 3. Transverse momentum distributions of the $t\bar{t}$ system, normalised. Left: interference contributions from σ_i . Right: squared contributions σ_{ii} . SM contributions and individual operator contributions are displayed. Lower panels give the K factors and $\mu_{R,F}$ uncertainties.

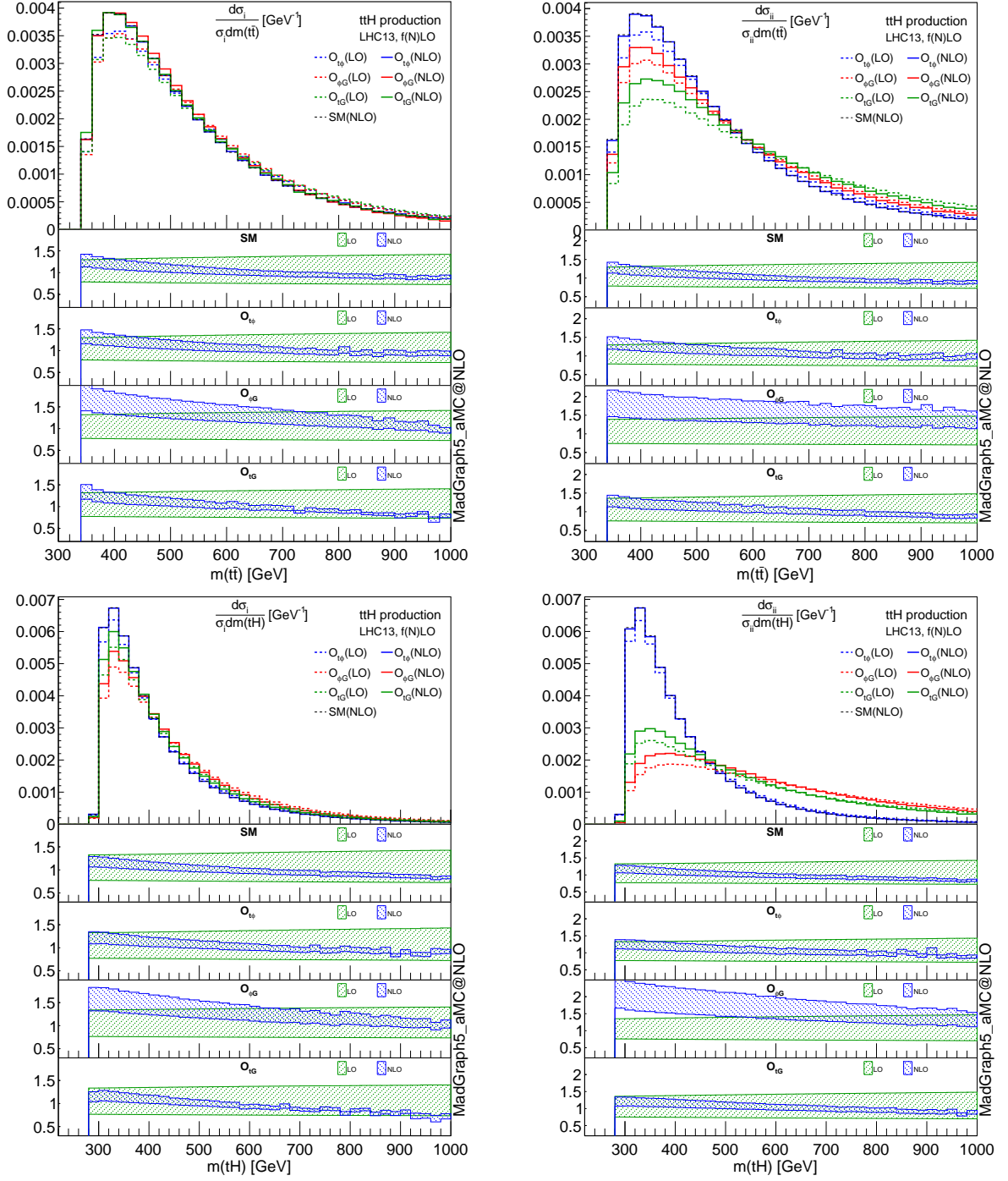


Figure 4. Invariant mass distributions of the $t\bar{t}$ system (up) and the $t + H$ system (down), normalised. Left: interference contributions from σ_i . Right: squared contributions σ_{ii} . SM contributions and individual operator contributions are displayed. Lower panels give the K factors and $\mu_{R,F}$ uncertainties.

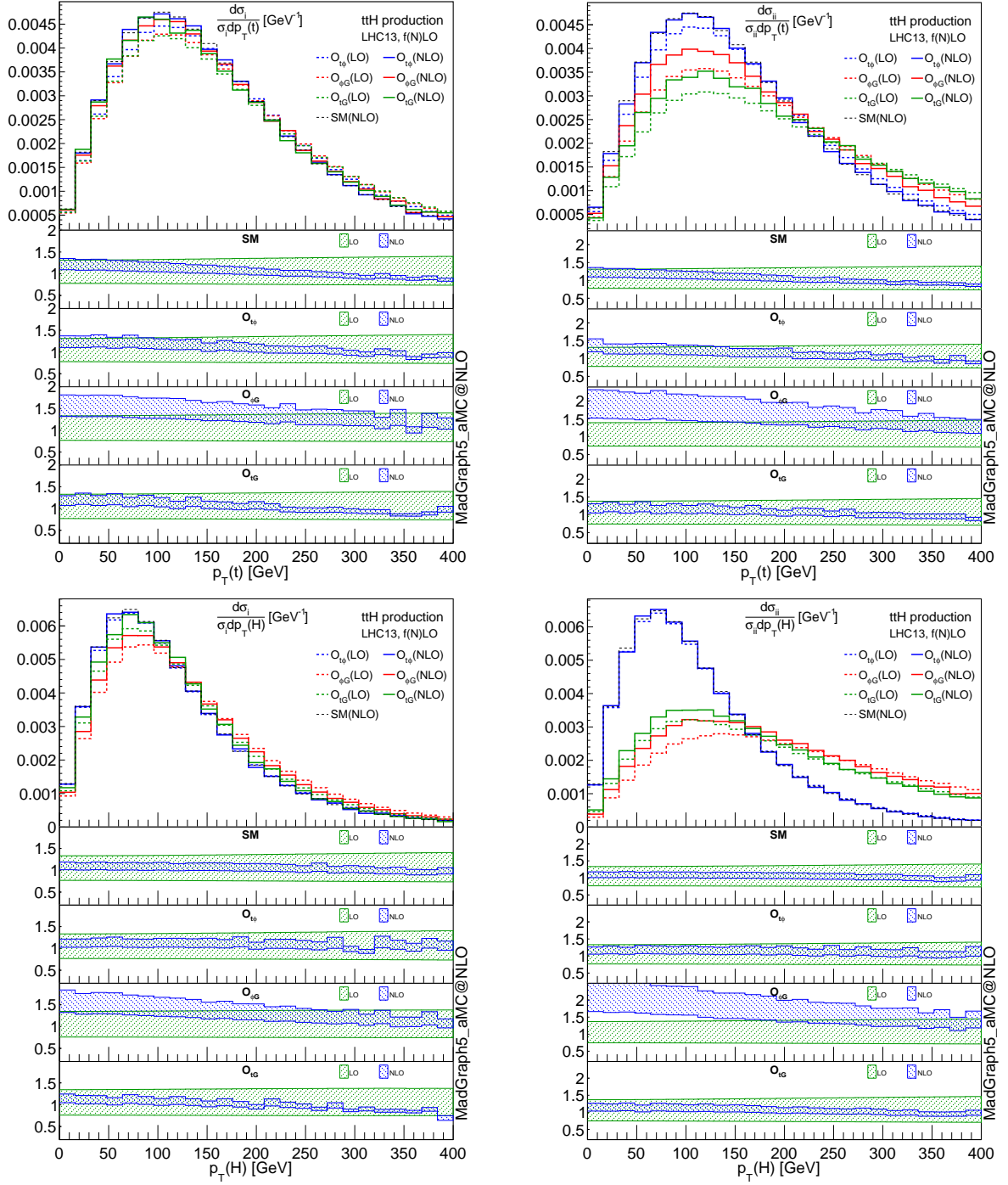


Figure 5. Transverse momentum distributions of the top quark (up) and the Higgs boson (down), normalised. Left: interference contributions from σ_i . Right: squared contributions σ_{ii} . SM contributions and individual operator contributions are displayed. Lower panels give the K factors and $\mu_{R,F}$ uncertainties.

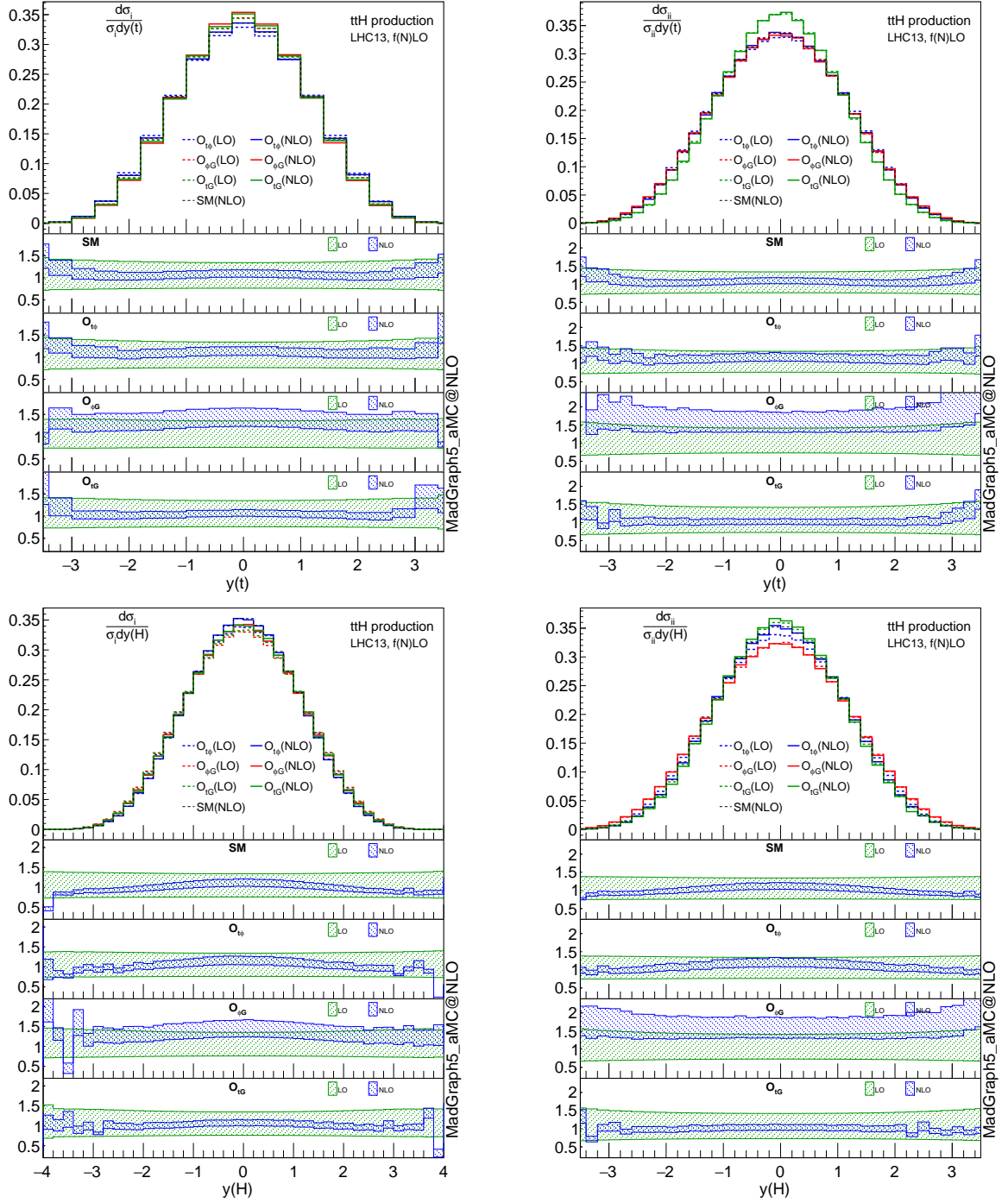


Figure 6. Rapidity distributions of the top quark (up) and the Higgs boson (down), normalised. Left: interference contributions from σ_i . Right: squared contributions σ_{ii} . SM contributions and individual operator contributions are displayed. Lower panels give the K factors and $\mu_{R,F}$ uncertainties.

$C_{tG} = \pm 1$ in Figure 7, and one can see that in particular $C_{tG} = 1$ leads to a very large deviation. In most cases, QCD corrections lead to nontrivial K factors that are not flat and can depend on operators, and using the SM K factor is not a good approximation. These corrections change the shapes of differential distribution, and missing such corrections could lead to bias in a fit where differential information is used.

The corresponding distributions for the Higgs and jet transverse momentum and Higgs rapidity in Hj are shown in Figures 8-10, where a 100 GeV cut has been imposed at parton level on the Higgs transverse momentum. Both the linear and the quadratic terms are shown. The corresponding scale uncertainty bands and the ratio over the SM with its scale uncertainty are also shown in the lower panels.

The $O_{\phi G}$ and O_{tG} give contributions which rise at high p_T , in particular the squared contributions, while $O_{t\phi}$ just gives rise to shapes identical to those of the SM. We note that the scale uncertainties in the ratio over the SM are extremely small for $O_{t\phi}$ and O_{tG} , and therefore not visible in the plots, while for $O_{\phi G}$ they are larger as we have also seen at the total cross-section level in Table 5.

The results for the Higgs pair invariant mass and hardest Higgs p_T in $pp \rightarrow HH$ are shown in Figure 11. All operators lead to shapes which differ from the SM, with the squared contributions leading to distributions rising fast with the energy. We find that the interference for $O_{\phi G}$ and O_{tG} can be destructive or constructive depending on the region of the phase space.

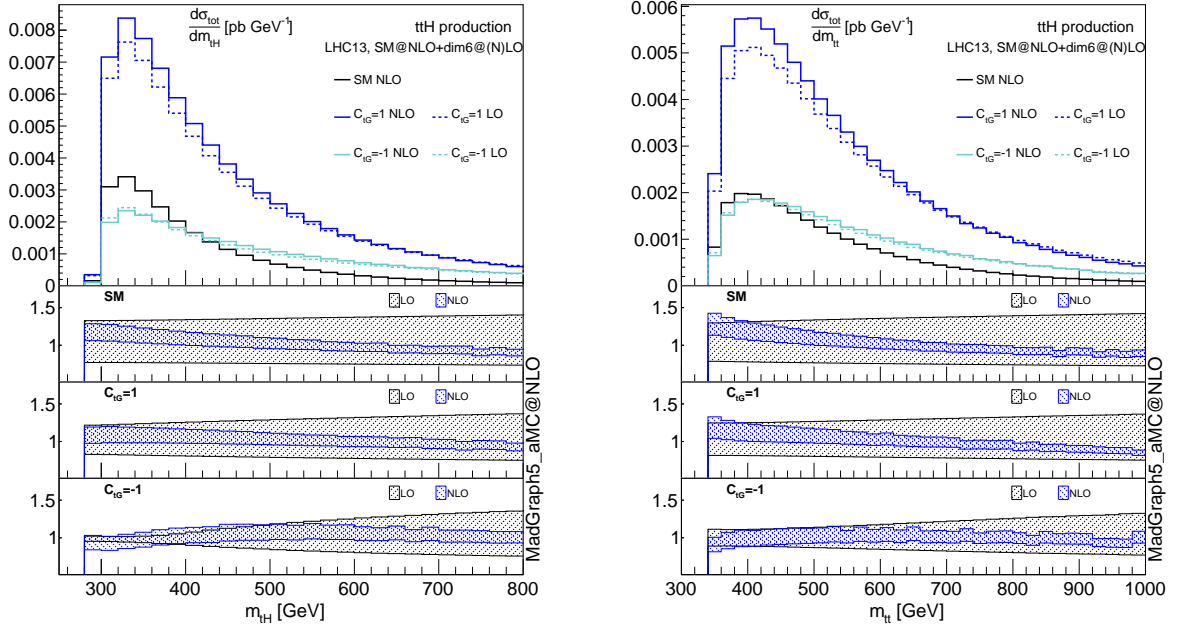


Figure 7. Left: invariant mass distributions of $t + H$ system. Right: invariant mass distributions of the top-pair system. Results are displayed for different values of C_{tG} , assuming $\Lambda = 1$ TeV. Lower panels give the K factors and $\mu_{R,F}$ uncertainties.

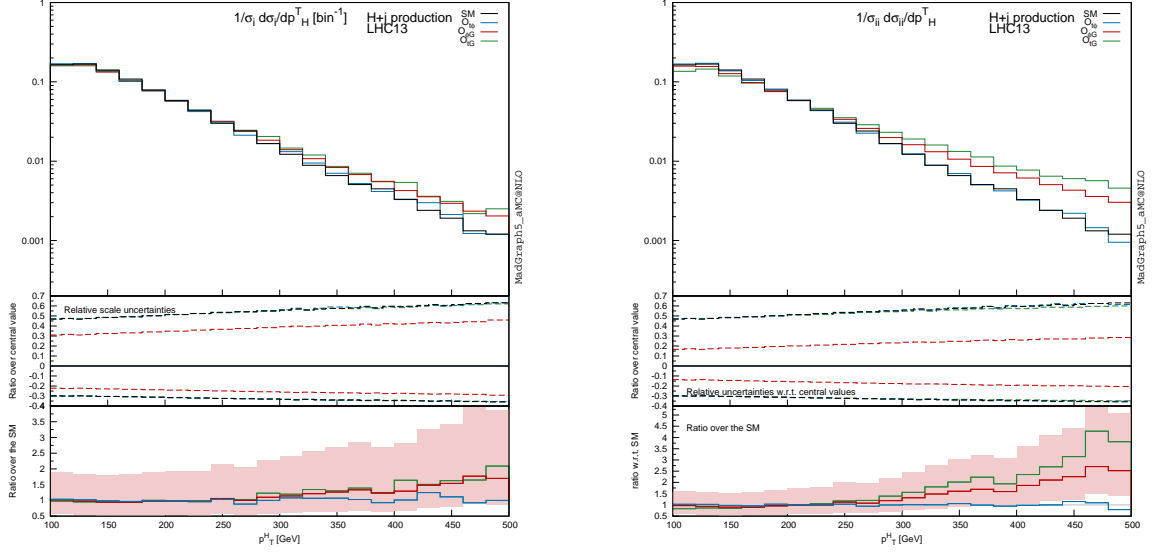


Figure 8. Higgs transverse momentum distribution in Hj , normalised. Left: Interference contribution from σ_i . Right: Squared contribution σ_{ii} . The SM and individual operator contributions are shown. Lower panels give the $\mu_{R,F}$ uncertainties and the ratio over the SM.

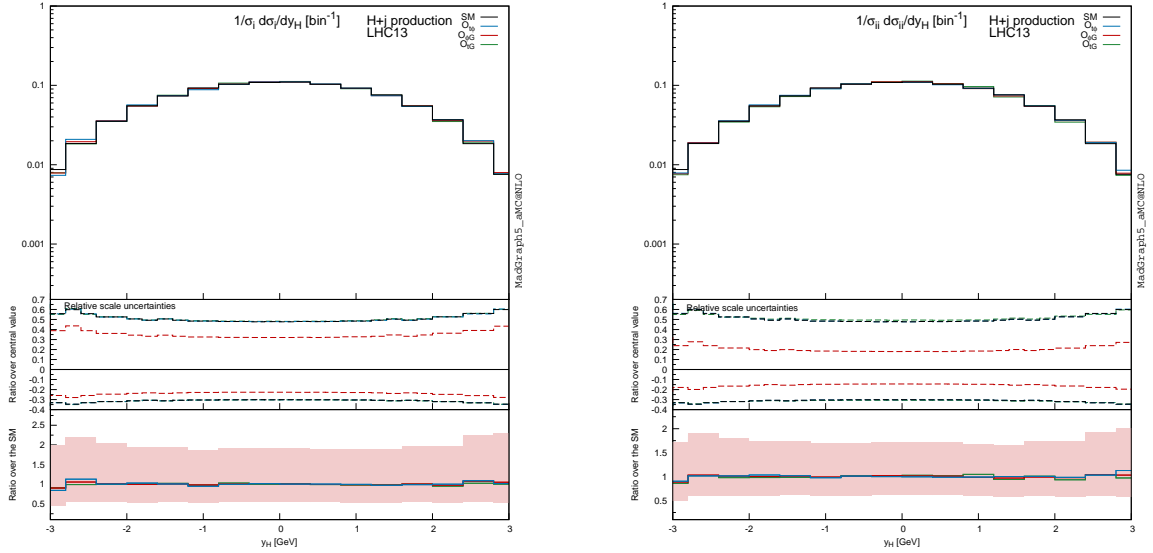


Figure 9. Higgs rapidity distribution in Hj , normalised. Left: Interference contribution from σ_i . Right: Squared contribution σ_{ii} . The SM and individual operator contributions are shown. Lower panels give the $\mu_{R,F}$ uncertainties and the ratio over the SM.

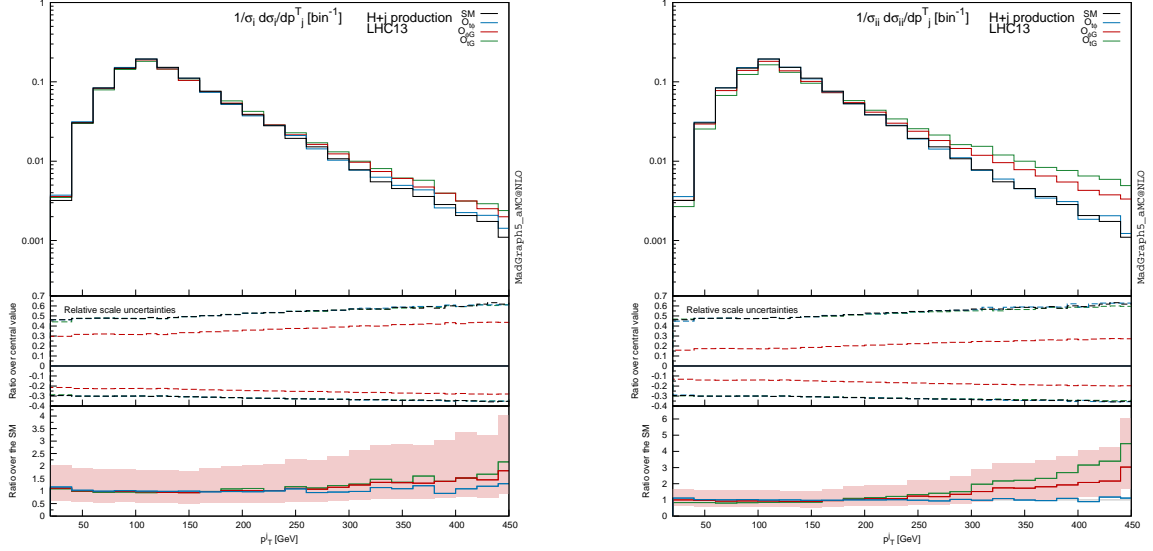


Figure 10. Transverse momentum distribution of the hardest jet in Hj , normalised. Left: Interference contribution from σ_i . Right: Squared contribution σ_{ii} . The SM and individual operator contributions are shown. Lower panels give the $\mu_{R,F}$ uncertainties and the ratio over the SM.

6 RG effects

In an NLO calculation in the SMEFT, the logarithmic dependence on μ_{EFT} arises as a consequence of the running and mixing effects among dimension-six operators. These terms are very important for correctly interpreting the NLO results, for extracting reliable constraints from an experimental analysis, and for estimating the theoretical uncertainties due to missing higher orders. On the other hand, in general, they do not provide an approximation of the complete NLO corrections. Many discussions on these issues are available in the literature and we refer the reader to, e.g., Refs. [48, 50, 105–107, 110].

In this section, we present a study of the RG effects using our NLO calculation as a concrete example. In particular, we focus on the role of RG effects in a full NLO calculation, and on their use in the estimate of missing higher-order corrections. The impact of the μ_{EFT} dependence on the extraction of experimental constraints is further discussed in Section 7.

Comparing RG corrections with full NLO

By naive power counting one might think that in an NLO calculation RG corrections to operators dominate over the finite pieces, as they are enhanced by factors of $\log(\Lambda/Q)$, where Q is a relatively low energy scale, at which the measurement is performed. This statement is not accurate. First, a measurement at scale Q is designed to measure parameters defined at that same scale, i.e. $C(Q)$, so in practice $\log(\Lambda/Q)$ will never appear in a perturbative

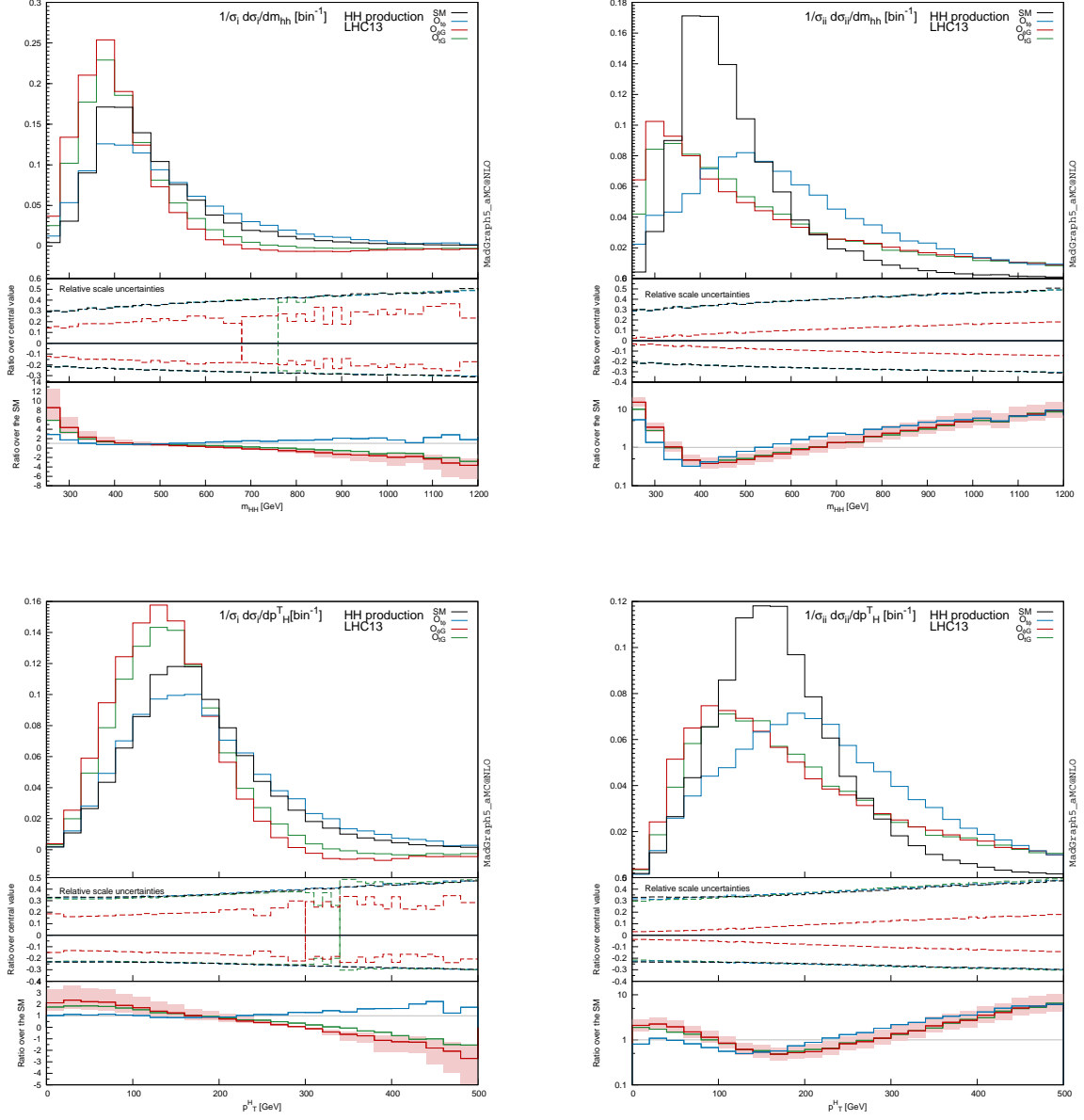


Figure 11. Higgs pair Invariant mass distribution (top) and transverse momentum distribution of the hardest Higgs (bottom) in $pp \rightarrow HH$, normalised. Left: Interference contribution from σ_i . Right: Squared contribution σ_{ii} . The SM and individual operator contributions are shown. Lower panels give the $\mu_{R,F}$ uncertainties and the ratio over the SM.

expansion. Rather, these log terms are resummed by using RG equations, independent of processes, so they are not part of an NLO calculation, but are contained in the definition of coefficients. The large logarithmic terms will play a role only if one wants to relate coefficients with underlying models, which is not the task of an NLO calculation in the

EFT.

Even if we do not resum these log terms, by setting $\mu_{EFT} = \Lambda$ explicitly in a perturbative calculation (which is looking for trouble and should not be done), the $\log(\Lambda/Q)$ terms appearing in the NLO corrections are often not the major contribution, because at the LHC QCD corrections are typically much larger than what one would naively estimate using $\mathcal{O}(\alpha_s/4\pi)$. It is interesting to compare the two kinds of corrections, i.e. RG and NLO, in the $t\bar{t}H$ process. In Figure 12 we show the interference contribution from three operators, $\sigma_i(\Lambda; \mu_{EFT})$ (i.e. contributions from $C_i(\Lambda)$, calculated with μ_{EFT}) for $\Lambda = 2$ TeV. Suppose we have an underlying theory which we match to an EFT at scale Λ with three coefficients $C_{t\phi}$, $C_{\phi G}$ and C_{tG} . We can do a LO calculation without running, and we normalize the results to one. Now we may use the RG equations to improve the results, by running the coefficients to a lower scale near m_t . The dashed lines indicate corrections from one-loop RG only. These corrections ranges from roughly 0 to 40%. However if we go to NLO, the increase is much larger, depending on where the scale is, as indicated by the solid lines. This clearly demonstrates that RG corrections are far from a good approximation to NLO corrections.

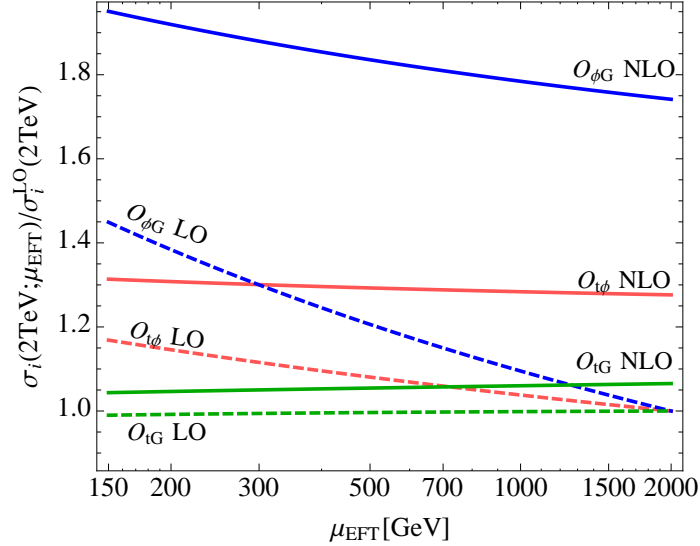


Figure 12. Comparison of the RG corrections with the exact NLO results for $t\bar{t}H$ production.

EFT scale as an uncertainty estimator

The RG running can still be used as an estimator of missing higher order corrections to the operators. From Figure 12 we can see that the EFT scale dependence of the LO results roughly captures the NLO corrections at the same order of magnitude. On the other hand, at NLO the EFT scale dependence becomes much smaller, indicating that the EFT scale uncertainty can be taken under control by using the full NLO prediction.

The curves in Figure 12 take into account both running and mixing effects. For example, as O_{tG} runs down, it will also mix into $O_{t\phi}$ and $O_{\phi G}$, and the green curves are the sum of

all three contributions. It is this sum that becomes less dependent on scales at NLO. The individual contribution from each operator is however not physical, in particular in loop induced processes, where the separation between tree-level and loop-level contributions from two different operators is scale dependent. For this reason, loop-induced contributions are sensitive to μ_{EFT} and should be used with care when setting bounds on individual operators. This will be further discussed in the following section where we set constraints on the operators.

For illustration, in Figure 13 we plot the individual contributions from the three operators in $pp \rightarrow H$ and $pp \rightarrow HH$, as a function of μ_{EFT} , assuming $C_{tG} = 1$, $C_{t\phi} = C_{\phi G} = 0$ at scale $\mu_{EFT} = m_t$, and $\Lambda = 1$ TeV. At this scale the only contribution is from O_{tG} . When μ_{EFT} deviates from m_t , while the running of C_{tG} is only at the percent level, its cross section has a strong μ_{EFT} dependence as can be seen from the “ $C_{tG}\sigma_{tG}$ ” curves; in the meantime, non-zero values for $C_{t\phi}$ and $C_{\phi G}$ are induced by O_{tG} , in particular the latter leading to a tree level contribution that also depends on μ_{EFT} , as can be seen from the “ $C_{\phi G}\sigma_{\phi G}$ ” curves. These dependences are canceled out at the leading log level when all three contributions are summed, as presented by the black curves labeled as “ $\sigma(\text{total})$ ”. This quantity is nothing but the $\sigma_{tG}(m_t; \mu_{EFT})$ defined in Eq. (4.5). It is the physical contribution coming from $C_{tG}(m_t) = 1$, and has a weaker dependence on μ_{EFT} between $m_t/2$ and $2m_t$. This quantity should be used as an estimation of the missing higher-order corrections to the effective operators, and should be presented in a perturbative EFT prediction, in the same way as the normal $\mu_{R,F}$ uncertainties are usually given.

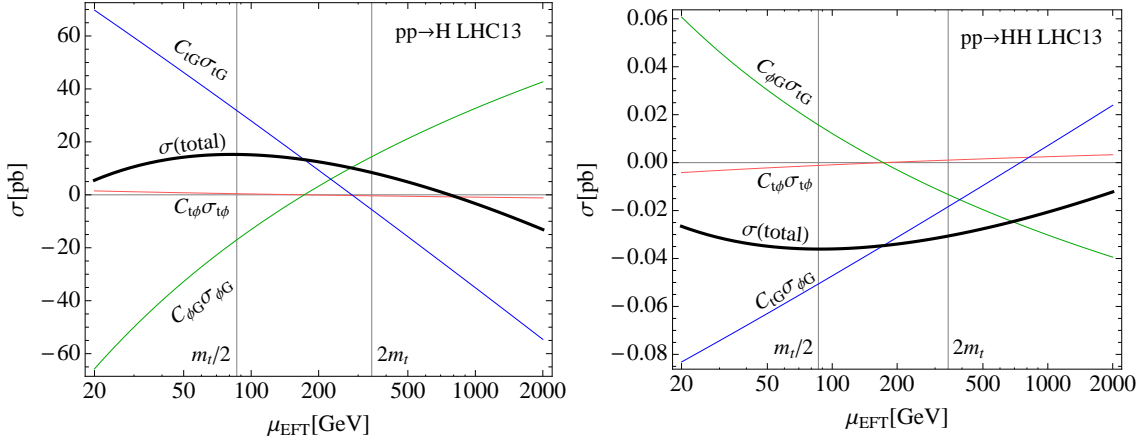


Figure 13. O_{tG} contribution in loop-induced processes, assuming $C_{tG}(m_t) = 1$, $C_{t\phi}(m_t) = C_{\phi G}(m_t) = 0$, and $\Lambda = 1$ TeV. Left: $pp \rightarrow H$. Right: $pp \rightarrow HH$. Individual linear contributions from each operator, as well as their sum, i.e. $\sigma_{tG}(m_t; \mu_{EFT})$, are displayed.

7 Constraints on dimension-six operators

In this section we study the experimental constraints on the operator coefficients. Both $pp \rightarrow H$ and $pp \rightarrow t\bar{t}H$ have been already measured at the LHC Run I. Even though the

latter is still not very accurate with the current integrated luminosity, we will see that it already provides useful information. In addition, Run II measurements for both processes at 13 TeV have started to appear, and we will also include them. The simple fit we will perform is however only for illustrative purposes, and therefore a number of simplifications and approximations are applied. The correlations of errors between different measurements due to common sources of uncertainties are ignored; uncertainties are always symmetrised by shifting the central values, and Gaussian distribution is assumed; theoretical uncertainties are included only for the production process. While we have shown results only for 8 TeV, we have checked that signal strengths at 7 TeV are identical, therefore we can use the measurements on signal strengths reported by experimental collaborations, where 7/8 TeV data are often combined. We also neglect the uncertainties due to missing dimension-eight and higher operators. These errors are estimated to be of order $[(2m_t + m_H)/\Lambda]^2$. The reliability of our results will thus depend on Λ , i.e. the scale of new physics, and can only be assessed as a function of Λ .

The $pp \rightarrow H$ measurements we are going to use are the following: in the diphoton channel we use [111, 112] at 8 TeV and [113] at 13 TeV; in $WW/ZZ/\tau\tau$ channels we use [114–119]; Measurements of $pp \rightarrow t\bar{t}H$ at 8 TeV in the diphoton channel are given in [30, 31], while in the multilepton and $b\bar{b}$ channels we use [30, 32, 33]. Finally, 13 TeV measurements of $t\bar{t}H$ in the multilepton and $b\bar{b}$ channels are also included [34, 35]. Both processes depend on all three operators.

$r_{t\phi}$	$r_{\phi G}$	r_{tG}	$r_{t\phi,t\phi}$	$r_{\phi G,\phi G}$	$r_{tG,tG}$	$r_{t\phi,\phi G}$	$r_{t\phi,tG}$	$r_{\phi G,tG}$
-0.119	73.4	0.676	0.00354	1348	0.114	-4.37	-0.0402	24.8

Table 6. Ratio of partial Higgs width into gg over the SM value, defined as: $\Gamma(gg)/\Gamma_{SM}(gg) \equiv 1 + \sum_i \frac{1\text{TeV}^2}{\Lambda^2} C_i r_i + \sum_{i \leq j} \frac{1\text{TeV}^4}{\Lambda^4} C_i C_j r_{ij}$.

The Higgs branching ratios are affected by the operators in different ways. As an example we show in Table 6 how the Higgs partial decay width to gluons changes for the relevant operators. In addition to $H \rightarrow gg$, $O_{t\phi}$ changes the partial width of the $H \rightarrow \gamma\gamma$ decay in the following way:

$$\frac{\Gamma(\gamma\gamma)}{\Gamma_{SM}(\gamma\gamma)} = \left| 1 - 0.0595 C_{t\phi} \frac{1\text{TeV}^2}{\Lambda^2} \frac{A_t}{A_t + A_W} \right|^2 = \left| 1 + 0.0335 \frac{1\text{TeV}^2}{\Lambda^2} C_{\phi t} + 0.000281 \frac{1\text{TeV}^4}{\Lambda^4} C_{\phi t}^2 \right|, \quad (7.1)$$

where A_t and A_W are the top- and W -boson loop amplitudes entering the Higgs decay into photons. We note that the impact of $O_{t\phi}$ is diluted in $H \rightarrow \gamma\gamma$ as this decay is dominated by the W -boson loop. All branching ratios, including those of $WW/ZZ/\tau\tau$, are also affected due to changes in the total width from $H \rightarrow gg$. We include these effects at LO only (tree-level for $O_{\phi G}$, one-loop for $O_{t\phi}$ and O_{tG}). For this reason different decay channels need to be considered separately. Because the measurements are based on signal strengths, defined as the ratio of deviation in cross sections to the SM prediction, we prefer to have same order predictions for both the SM and operator contributions. For $t\bar{t}H$ we use our NLO predictions, while for $pp \rightarrow H$ and Higgs decay we only use LO predictions,

	Individual	Marginalised	C_{tG} fixed
$C_{t\phi}/\Lambda^2$ [TeV $^{-2}$]	[-3.9,4.0]	[-14,31]	[-12,20]
$C_{\phi G}/\Lambda^2$ [TeV $^{-2}$]	[-0.0072,-0.0063]	[-0.021,0.054]	[-0.022,0.031]
C_{tG}/Λ^2 [TeV $^{-2}$]	[-0.68,0.62]	[-1.8,1.6]	

Table 7. Constraints on C/Λ^2 from the simplified fit. In the first column, only one operator is allowed at a time. In the second column, all operator coefficients are allowed to float. In the third column, C_{tG} is set to zero while the other two coefficients are floated.

as not all loop-induced contributions are known at NLO. Both production and decay rates are included up to order C^2/Λ^4 . A χ^2 -fit is performed to derive the limits. All coefficients in this section are defined with $\mu_{EFT} = m_t$ unless specifically mentioned, and all results given in this section correspond to 95% confidence level.

Top-pair production is not included in the fit. We assume that this degree of freedom will be used to constrain the four-fermion operators. While a global fit including both sectors is the only consistent way to extract information on the dimension-six operators, this is beyond the scope of this paper.

Current limits at 95% confidence level are given in Table 7. The most constrained operator is $C_{\phi G}$, as it gives a tree-level contribution to Higgs production. Individual limits (i.e. setting other coefficients to zero) and marginalised ones (i.e. floating other coefficients) are given in the first two columns. Interestingly, the C_{tG} limit is already comparable to its current limit from $t\bar{t}$ production only (assuming no four-fermion operator contributes). This is because the $t\bar{t}H$ cross section is more sensitive to the O_{tG} operator due to the higher partonic energies probed, and in addition the squared contribution from C_{tG} given the current limits is not negligible. Even though the current limit from $t\bar{t}H$ is still weaker, given that the $t\bar{t}H$ measurement still has a lot of room to improve, it will become more competitive in the near future. In fact, assuming 10% uncertainty on $t\bar{t}H$ and 4% uncertainty on $pp \rightarrow H$ for 14 TeV 3000 fb $^{-1}$ [36], we find $-0.12 < C_{tG} < 0.12$ and $-1.0 < C_{tG} < 1.1$ ($\Lambda = 1$ TeV) respectively for individual and marginalised limits. On the other hand, assuming a 5% precision for $t\bar{t}$ production at 14 TeV, the individual limit on C_{tG} is $-0.33 < C_{tG} < 0.33$ ($\Lambda = 1$ TeV) [43], and a factor of a few is expected once marginalised over the four-fermion operators.

In the third column of Table 7 we show limits obtained by assuming only $C_{tG} = 0$ but floating the other two coefficients. $C_{tG} = 0$ is typically assumed in Higgs operator analyses. By comparing the last two columns in the table, we can see how much more room is allowed once this operator is included.

We should also point out that, given the cross sections in Table 1 and the limits in Table 7, in $t\bar{t}H$ production the squared contribution from $O_{\phi G}$ is negligible, but that from the other two operators cannot be neglected.

As we have mentioned in the previous section, limits on operator coefficients can be sensitive to the EFT scale. In Figure 14 we plot the individual and marginalised bounds on the three operator coefficients as in Table 7, but this time as a function of μ_{EFT} . We can see that the individual bound on C_{tG} has a large dependence on scales, and does not provide

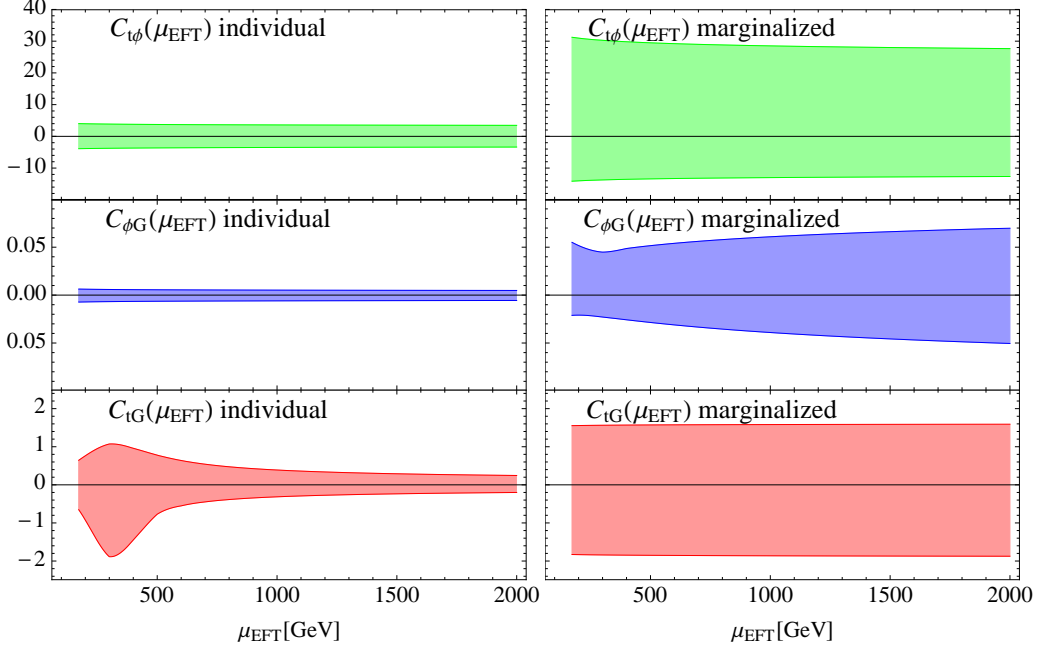


Figure 14. Individual (left) and marginalised (right) limits on the three operator coefficients, as functions of μ_{EFT} . $\Lambda = 1$ TeV is assumed.

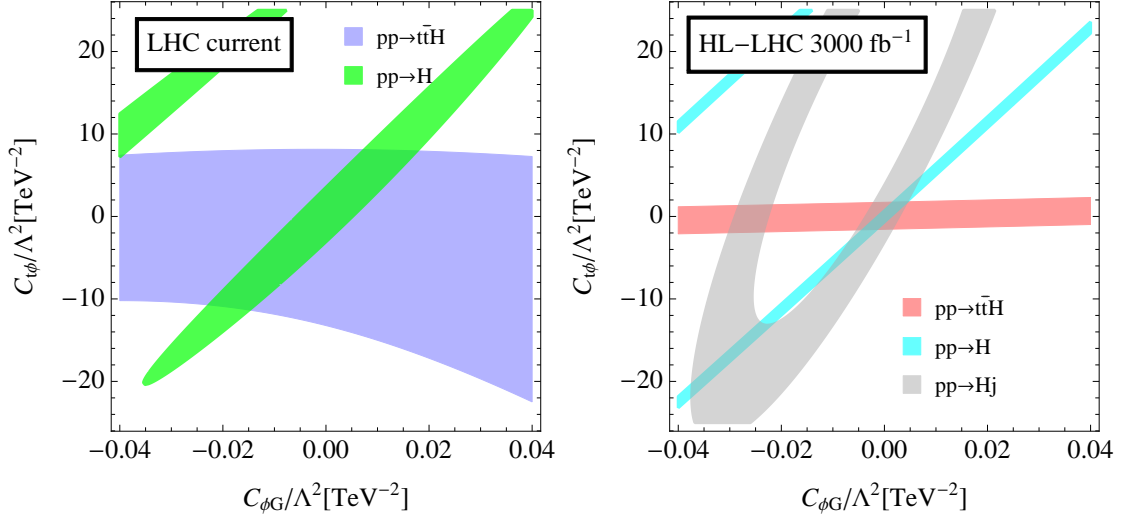


Figure 15. Allowed region in $O_{t\phi}$ - $O_{\phi G}$ plane at 95% confidence level. Left: current constraints. Right: future projection at HL-LHC.

valuable information. This is because the bounds are derived by assuming $C(\mu_{EFT}) = 0$ for the other two operators, which is a scale-dependent assumption. The marginalised bounds are more stable because they are independent of such assumptions.

To better investigate the allowed region in the parameter space, in the following we

consider scenarios where two operators are allowed at a time. Particularly interesting is the degeneracy of the three operators in $gg \rightarrow H$. Through a top-quark loop, both $O_{t\phi}$ and O_{tG} can induce a ggH vertex, leading to a degeneracy with the tree-level contribution of $O_{\phi G}$. $t\bar{t}H$ production is expected to break this degeneracy. To illustrate this effect, we make plots to compare the constraints from the two processes, each time allowing two operators to be nonzero.

We first consider the degeneracy between $O_{t\phi}$ and $O_{\phi G}$. In Figure 15 left we show limits obtained from $pp \rightarrow H$ and $pp \rightarrow t\bar{t}H$ separately. We can see the flat direction in the $pp \rightarrow H$ measurement is already slightly lifted. This is due to including branching ratios of the diphoton and other channels, which have different dependence on $O_{t\phi}$ and $O_{\phi G}$. On the other hand, the current measurement of $t\bar{t}H$ cross section gives constraints in the orthogonal direction. Even though the precision is still not comparable to the Higgs cross section measurement, improvements can be expected in the future. For illustration, in Figure 15 right we show the 14 TeV projections for 3000 fb⁻¹. For simplicity we only consider the production processes. Estimated experimental uncertainties on both $pp \rightarrow t\bar{t}H$ and $pp \rightarrow H$ are taken from [36]. Theoretical uncertainties are not included.

Another useful process to break this degeneracy is $pp \rightarrow Hj$ with a boosted Higgs, as suggested in Ref. [82]. For this reason we also include this process in Figure 15 right. As an estimation for future precision, Ref. [82] considered a $p_T(j)$ cut of 650 GeV and 10% uncertainty on the measurement. A large $p_T(j)$ significantly reduces the cross section, and to be more conservative, here we consider $p_T(j) > 500$ GeV and assign a 20% uncertainty on the measurement. We can see that the limit range from this measurement does cross the $pp \rightarrow H$ region as expected, so there is some discriminating power. The direction is however not very “orthogonal”, and so the discriminating power with our assumption is not as good as $t\bar{t}H$, even though a more detailed analysis would be needed to draw a final conclusion.

The degeneracy between O_{tG} and $O_{\phi G}$, i.e. $t\bar{t}g$ and ggH vertices, has been less considered in the literature [68], mainly because O_{tG} is expected to be constrained from $t\bar{t}$ production. However as we have mentioned, considering future measurements, $t\bar{t}H$ will become sensitive to O_{tG} in its limited range, and a more reasonable strategy could be to use $t\bar{t}$ to constrain four-fermion operators while leaving O_{tG} to $t\bar{t}H$ production. For this reason, we plot in Figure 16 left the current limits from $pp \rightarrow H$ and $pp \rightarrow t\bar{t}H$. Including Higgs decays will not lift the degeneracy in this case, but we see that $t\bar{t}H$ production already gives a useful bound on O_{tG} . Projections for 14 TeV 3000 fb⁻¹ are shown in Figure 16 right. The expected limit on C_{tG} is improved. We can also see that $pp \rightarrow Hj$ does not provide additional information in resolving O_{tG} and $O_{\phi G}$.

Unlike $O_{t\phi}$, the contributions from O_{tG} and $O_{\phi G}$ are sensitive to the scale μ_{EFT} , because the top loop with an O_{tG} insertion is divergent and requires a counterterm from $O_{\phi G}$. As a result, the dependence of $C_{\phi G}$ on μ_{EFT} due to mixing from C_{tG} is expected to be canceled by the μ_{EFT} dependence in the loop. When the scale μ_{EFT} is changed, the change in total cross section is only a higher order effect, but the contours in the $C_{tG} - C_{\phi G}$ plot will be very different, as we can see by comparing with the 95% contours in Figure 17 at two different μ_{EFT} scales, $2m_t$ and 1 TeV. It is therefore very important to give the value of μ_{EFT} when presenting bounds on operators. As we can see by comparing the left plots of Figures 16

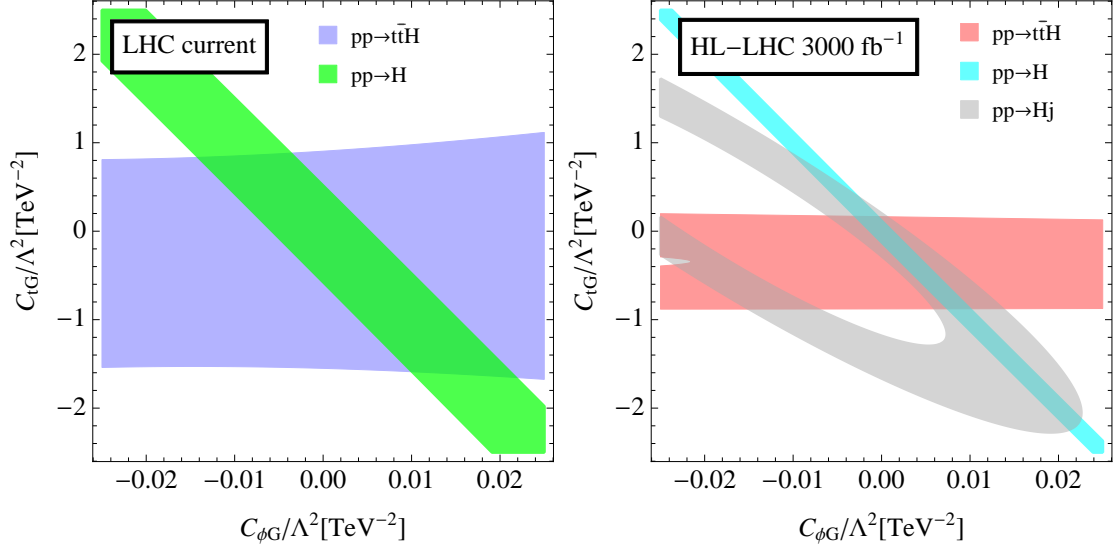


Figure 16. Allowed region in O_{tG} - $O_{\phi G}$ plane at 95% confidence level. Left: current constraints. Right: future projection at HL-LHC.

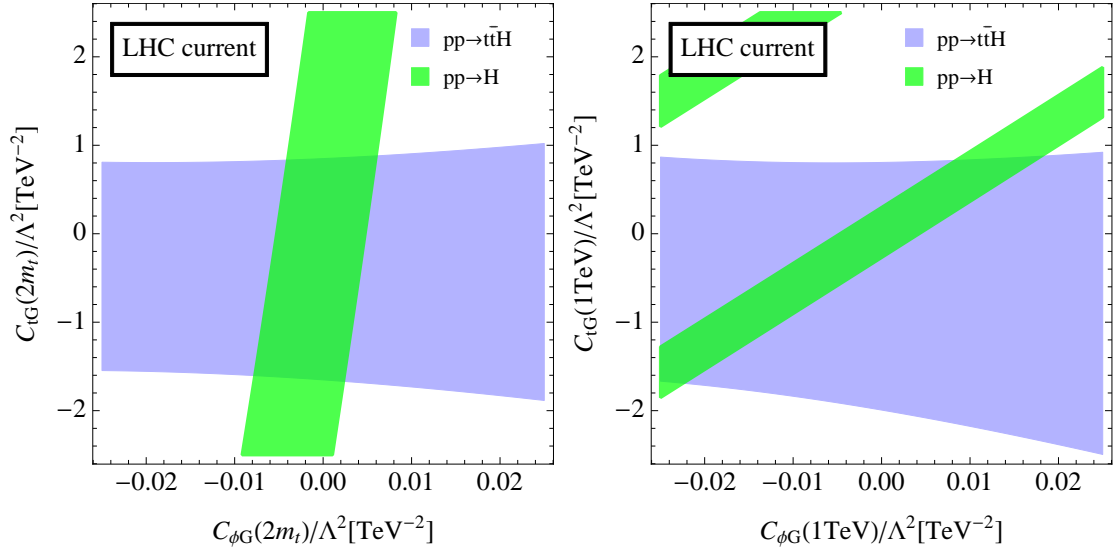


Figure 17. Allowed region in O_{tG} - $O_{\phi G}$ plane at 95% confidence level, setting $\mu_{EFT} = 2m_t$ (left) and $\mu_{EFT} = 1$ TeV (right).

and 17, even a change by a factor of two can lead to significant difference. In particular if $C_{\phi G}$ is set to 0 to derive the “individual bound” on C_{tG} , the result can be very sensitive to the scale. This is also reflected in Figure 14. We conclude that the “individual bound” in this case does not provide useful information.

Finally in figure 18 we show a two operator fit for $O_{t\phi}$ and O_{tG} , both giving loop-induced contribution in $pp \rightarrow H$. Figure 18 left shows how the current $t\bar{t}H$ measurements

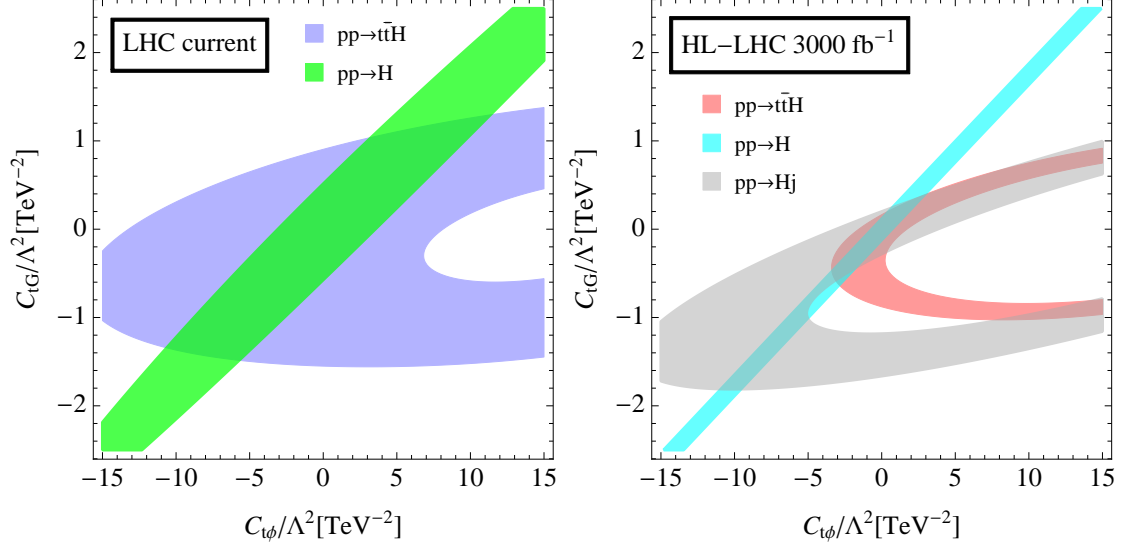


Figure 18. Allowed region in O_{tG} - $O_{t\phi}$ plane at 95% confidence level. Left: current constraints. Right: future projection at HL-LHC.

help to constrain both operators, while Figure 18 right is the situation for future LHC, where one can see that $t\bar{t}H$ and Hj are equally good in resolving the degeneracy between the two loop-induced contributions.

8 Summary and conclusions

We have presented the QCD NLO predictions for $t\bar{t}H$ production, as well as results for several other loop-induced processes, H , Hj , HH production, all in the SMEFT. We have focused on the Yukawa operator, $O_{t\phi}$, the operator describing the interaction of gluons with the Higgs, $O_{\phi G}$, and the chromomagnetic dipole moment O_{tG} . Our predictions improve our understanding of the patterns of deviations from the SM in both the top-quark and the Higgs-boson sectors, and will play an important role in future measurements of these two sectors.

We have shown that the QCD corrections to the $t\bar{t}H$ improve both the accuracy and the precision, and in many cases lead to nontrivial modification of the distributions of relevant observables. K factors for the inclusive cross sections range roughly from 1 to 1.6, depending on the effective operator. Moreover, the differential K factors are not a constant and their shapes also depend on the operator. Using the SM K factor to rescale the operator contribution may not be a good approximation. We have also shown that the full NLO corrections in $t\bar{t}H$ can be much larger than only the log enhanced terms which are captured by RG equations, so the RG-improved prediction is not a good approximation to the full NLO prediction.

To assess the sensitivity of the various Higgs production mechanisms to the dimension-six operators, we have performed a toy fit for the three effective operators $O_{t\phi}$, $O_{\phi G}$ and

O_{tG} , using $t\bar{t}H$ production and $pp \rightarrow H$. The projection at HL-LHC is also discussed, together with $pp \rightarrow H j$. We find that the current limit on C_{tG} is already comparable, even though still weaker, to the limit obtained directly from $t\bar{t}$ production, and that in the future $t\bar{t}H$ and $pp \rightarrow H$ could be a better approach to set limits on this coupling. This implies that the Higgs measurements have started to become sensitive to the chromo-dipole coupling of the top, and so this should be included in future Higgs analysis. Furthermore, the ratio between $t\bar{t}H$ and $t\bar{t}$ measurements is useful in decoupling the impact of potential four-fermion operator contributions. We have also shown how the $t\bar{t}H$ and $H j$ production processes can be used to resolve the degeneracy between the three operators in the $pp \rightarrow H$ measurement.

We have further discussed the EFT scale dependence, that is, the scale at which the EFT is defined, in an operator analysis. For example we show that individual bounds could have a strong dependence on this scale, and so should always be interpreted with care. This is because loop-induced processes can be sensitive to the EFT scale even at LO, and the dependence is supposed to be canceled by RG mixing effects. In addition we have defined a way to estimate the scale uncertainty induced by this additional scale, which properly takes into account the RG mixing and running, and showed that with our NLO results this uncertainty can be put under control. The EFT predictions should always be presented with this uncertainty.

In summary, at NLO in QCD accuracy deviations from the SM in the top and the Higgs sectors can be extracted with improved accuracy and precision, allowing for more reliable global analyses based on the EFT approach. Similar to our previous works, these results are performed with the MG5_AMC framework, and predictions matched to the PS are provided in an automatic way. For this reason NLO+PS event generation can be directly used in a realistic simulation, and by investigating the features of potential deviations from SM, sensitivities to EFT signals will possibly be improved with advanced experimental techniques.

Acknowledgments

We are grateful to the LHCHXSWG for always providing us with such a stimulating environment. We acknowledge many illuminating discussions on EFT at NLO with Celine Degrande, Christophe Grojean and Giampiero Passarino. This work has been performed in the framework of the ERC Grant No. 291377 “LHCTheory” and has been supported in part by the European Union as part of the FP7 Marie Curie Initial Training Network MCnetITN (PITN-GA-2012-315877). C.Z. is supported by the United States Department of Energy under Grant Contracts DE-SC0012704.

References

- [1] D. Buttazzo, G. Degrassi, P. P. Giardino, G. F. Giudice, F. Sala, A. Salvio et al., *Investigating the near-criticality of the Higgs boson*, *JHEP* **12** (2013) 089, [[1307.3536](#)].
- [2] F. Maltoni, K. Paul, T. Stelzer and S. Willenbrock, *Associated production of Higgs and single top at hadron colliders*, *Phys. Rev.* **D64** (2001) 094023, [[hep-ph/0106293](#)].

- [3] M. Farina, C. Grojean, F. Maltoni, E. Salvioni and A. Thamm, *Lifting degeneracies in Higgs couplings using single top production in association with a Higgs boson*, *JHEP* **05** (2013) 022, [[1211.3736](#)].
- [4] F. Demartin, F. Maltoni, K. Mawatari and M. Zaro, *Higgs production in association with a single top quark at the LHC*, *Eur. Phys. J.* **C75** (2015) 267, [[1504.00611](#)].
- [5] J. Ellis, D. S. Hwang, K. Sakurai and M. Takeuchi, *Disentangling Higgs-Top Couplings in Associated Production*, *JHEP* **04** (2014) 004, [[1312.5736](#)].
- [6] S. Khatibi and M. M. Najafabadi, *Exploring the Anomalous Higgs-top Couplings*, *Phys. Rev.* **D90** (2014) 074014, [[1409.6553](#)].
- [7] F. Demartin, F. Maltoni, K. Mawatari, B. Page and M. Zaro, *Higgs characterisation at NLO in QCD: CP properties of the top-quark Yukawa interaction*, *Eur. Phys. J.* **C74** (2014) 3065, [[1407.5089](#)].
- [8] K. Kolodziej and A. Slapik, *Probing the top-Higgs coupling through the secondary lepton distributions in the associated production of the top-quark pair and Higgs boson at the LHC*, *Eur. Phys. J.* **C75** (2015) 475, [[1507.01572](#)].
- [9] M. R. Buckley and D. Goncalves, *Boosting the Direct CP Measurement of the Higgs-Top Coupling*, *Phys. Rev. Lett.* **116** (2016) 091801, [[1507.07926](#)].
- [10] M. L. Mangano, T. Plehn, P. Reimitz, T. Schell and H.-S. Shao, *Measuring the Top Yukawa Coupling at 100 TeV*, *J. Phys.* **G43** (2016) 035001, [[1507.08169](#)].
- [11] N. Moretti, P. Petrov, S. Pozzorini and M. Spannowsky, *Measuring the signal strength in $t\bar{t}H$ with $H \rightarrow b\bar{b}$* , *Phys. Rev.* **D93** (2016) 014019, [[1510.08468](#)].
- [12] Q.-H. Cao, S.-L. Chen and Y. Liu, *Probing Higgs Width and Top Quark Yukawa Coupling from $t\bar{t}H$ and $t\bar{t}t\bar{t}$ Productions*, [1602.01934](#).
- [13] V. Cirigliano, W. Dekens, J. de Vries and E. Mereghetti, *Constraining the top-Higgs sector of the Standard Model Effective Field Theory*, [1605.04311](#).
- [14] A. V. Gritsan, R. Röntsch, M. Schulze and M. Xiao, *Constraining anomalous Higgs boson couplings to the heavy flavor fermions using matrix element techniques*, [1606.03107](#).
- [15] W. Beenakker, S. Dittmaier, M. Kramer, B. Plumper, M. Spira and P. M. Zerwas, *Higgs radiation off top quarks at the Tevatron and the LHC*, *Phys. Rev. Lett.* **87** (2001) 201805, [[hep-ph/0107081](#)].
- [16] W. Beenakker, S. Dittmaier, M. Kramer, B. Plumper, M. Spira and P. M. Zerwas, *NLO QCD corrections to t anti- t H production in hadron collisions*, *Nucl. Phys.* **B653** (2003) 151–203, [[hep-ph/0211352](#)].
- [17] L. Reina and S. Dawson, *Next-to-leading order results for t anti- t h production at the Tevatron*, *Phys. Rev. Lett.* **87** (2001) 201804, [[hep-ph/0107101](#)].
- [18] L. Reina, S. Dawson and D. Wackeroth, *QCD corrections to associated t anti- t h production at the Tevatron*, *Phys. Rev.* **D65** (2002) 053017, [[hep-ph/0109066](#)].
- [19] S. Dawson, L. H. Orr, L. Reina and D. Wackeroth, *Associated top quark Higgs boson production at the LHC*, *Phys. Rev.* **D67** (2003) 071503, [[hep-ph/0211438](#)].
- [20] S. Dawson, C. Jackson, L. H. Orr, L. Reina and D. Wackeroth, *Associated Higgs production with top quarks at the large hadron collider: NLO QCD corrections*, *Phys. Rev.* **D68** (2003) 034022, [[hep-ph/0305087](#)].

- [21] R. Frederix, S. Frixione, V. Hirschi, F. Maltoni, R. Pittau and P. Torrielli, *Scalar and pseudoscalar Higgs production in association with a top-antitop pair*, *Phys. Lett.* **B701** (2011) 427–433, [[1104.5613](#)].
- [22] M. V. Garzelli, A. Kardos, C. G. Papadopoulos and Z. Trocsanyi, *Standard Model Higgs boson production in association with a top anti-top pair at NLO with parton showering*, *Europhys. Lett.* **96** (2011) 11001, [[1108.0387](#)].
- [23] A. Denner and R. Feger, *NLO QCD corrections to off-shell top-antitop production with leptonic decays in association with a Higgs boson at the LHC*, *JHEP* **11** (2015) 209, [[1506.07448](#)].
- [24] Y. Zhang, W.-G. Ma, R.-Y. Zhang, C. Chen and L. Guo, *QCD NLO and EW NLO corrections to $t\bar{t}H$ production with top quark decays at hadron collider*, *Phys. Lett.* **B738** (2014) 1–5, [[1407.1110](#)].
- [25] S. Frixione, V. Hirschi, D. Pagani, H. S. Shao and M. Zaro, *Weak corrections to Higgs hadroproduction in association with a top-quark pair*, *JHEP* **09** (2014) 065, [[1407.0823](#)].
- [26] S. Frixione, V. Hirschi, D. Pagani, H. S. Shao and M. Zaro, *Electroweak and QCD corrections to top-pair hadroproduction in association with heavy bosons*, *JHEP* **06** (2015) 184, [[1504.03446](#)].
- [27] H. B. Hartanto, B. Jager, L. Reina and D. Wackerroth, *Higgs boson production in association with top quarks in the POWHEG BOX*, *Phys. Rev.* **D91** (2015) 094003, [[1501.04498](#)].
- [28] A. Kulesza, L. Motyka, T. Stebel and V. Theeuwes, *Soft gluon resummation for associated $t\bar{t}H$ production at the LHC*, *JHEP* **03** (2016) 065, [[1509.02780](#)].
- [29] A. Broggio, A. Ferroglia, B. D. Pecjak, A. Signer and L. L. Yang, *Associated production of a top pair and a Higgs boson beyond NLO*, *JHEP* **03** (2016) 124, [[1510.01914](#)].
- [30] CMS collaboration, V. Khachatryan et al., *Search for the associated production of the Higgs boson with a top-quark pair*, *JHEP* **09** (2014) 087, [[1408.1682](#)].
- [31] ATLAS collaboration, G. Aad et al., *Search for $H \rightarrow \gamma\gamma$ produced in association with top quarks and constraints on the Yukawa coupling between the top quark and the Higgs boson using data taken at 7 TeV and 8 TeV with the ATLAS detector*, *Phys. Lett.* **B740** (2015) 222–242, [[1409.3122](#)].
- [32] ATLAS collaboration, G. Aad et al., *Search for the associated production of the Higgs boson with a top quark pair in multilepton final states with the ATLAS detector*, *Phys. Lett.* **B749** (2015) 519–541, [[1506.05988](#)].
- [33] ATLAS collaboration, G. Aad et al., *Search for the Standard Model Higgs boson produced in association with top quarks and decaying into $b\bar{b}$ in pp collisions at $\sqrt{s} = 8$ TeV with the ATLAS detector*, *Eur. Phys. J.* **C75** (2015) 349, [[1503.05066](#)].
- [34] CMS collaboration, *Search for $t\bar{t}H$ production in multilepton final states at $\sqrt{s} = 13$ TeV*, Tech. Rep. CMS-PAS-HIG-15-008, CERN, Geneva, 2016.
- [35] CMS collaboration, *Search for $t\bar{t}H$ production in the $H \rightarrow b\bar{b}$ decay channel with $\sqrt{s} = 13$ TeV pp collisions at the CMS experiment*, Tech. Rep. CMS-PAS-HIG-16-004, CERN, Geneva, 2016.
- [36] *Projections for measurements of Higgs boson signal strengths and coupling parameters with the ATLAS detector at a HL-LHC*, Tech. Rep. ATL-PHYS-PUB-2014-016, CERN, Geneva, Oct, 2014.

- [37] S. Weinberg, *Phenomenological Lagrangians*, *Physica* **A96** (1979) 327.
- [38] W. Buchmuller and D. Wyler, *Effective Lagrangian Analysis of New Interactions and Flavor Conservation*, *Nucl. Phys.* **B268** (1986) 621–653.
- [39] C. N. Leung, S. T. Love and S. Rao, *Low-Energy Manifestations of a New Interaction Scale: Operator Analysis*, *Z. Phys.* **C31** (1986) 433.
- [40] C. Zhang and F. Maltoni, *Top-quark decay into Higgs boson and a light quark at next-to-leading order in QCD*, *Phys.Rev.* **D88** (2013) 054005, [[1305.7386](#)].
- [41] C. Zhang, *Effective field theory approach to top-quark decay at next-to-leading order in QCD*, *Phys. Rev.* **D90** (2014) 014008, [[1404.1264](#)].
- [42] C. Degrande, F. Maltoni, J. Wang and C. Zhang, *Automatic computations at next-to-leading order in QCD for top-quark flavor-changing neutral processes*, *Phys. Rev.* **D91** (2015) 034024, [[1412.5594](#)].
- [43] D. Buarque Franzosi and C. Zhang, *Probing the top-quark chromomagnetic dipole moment at next-to-leading order in QCD*, *Phys. Rev.* **D91** (2015) 114010, [[1503.08841](#)].
- [44] C. Zhang, *Single Top Production at Next-to-Leading Order in the Standard Model Effective Field Theory*, *Phys. Rev. Lett.* **116** (2016) 162002, [[1601.06163](#)].
- [45] O. Bessidskaia Bylund, F. Maltoni, I. Tsirikos, E. Vryonidou and C. Zhang, *Probing top quark neutral couplings in the Standard Model Effective Field Theory at NLO in QCD*, *JHEP* **05** (2016) 052, [[1601.08193](#)].
- [46] R. Röntsch and M. Schulze, *Constraining couplings of top quarks to the Z boson in $t\bar{t} + Z$ production at the LHC*, *JHEP* **07** (2014) 091, [[1404.1005](#)].
- [47] R. Röntsch and M. Schulze, *Probing top-Z dipole moments at the LHC and ILC*, *JHEP* **08** (2015) 044, [[1501.05939](#)].
- [48] C. Hartmann and M. Trott, *On one-loop corrections in the standard model effective field theory; the $\Gamma(h \rightarrow \gamma\gamma)$ case*, *JHEP* **07** (2015) 151, [[1505.02646](#)].
- [49] M. Ghezzi, R. Gomez-Ambrosio, G. Passarino and S. Uccirati, *NLO Higgs effective field theory and κ -framework*, *JHEP* **07** (2015) 175, [[1505.03706](#)].
- [50] C. Hartmann and M. Trott, *Higgs Decay to Two Photons at One Loop in the Standard Model Effective Field Theory*, *Phys. Rev. Lett.* **115** (2015) 191801, [[1507.03568](#)].
- [51] R. Gauld, B. D. Pecjak and D. J. Scott, *One-loop corrections to $h \rightarrow b\bar{b}$ and $h \rightarrow \tau\bar{\tau}$ decays in the Standard Model Dimension-6 EFT: four-fermion operators and the large- m_t limit*, *JHEP* **05** (2016) 080, [[1512.02508](#)].
- [52] T. Corbett, O. J. P. Eboli, J. Gonzalez-Fraile and M. C. Gonzalez-Garcia, *Constraining anomalous Higgs interactions*, *Phys. Rev.* **D86** (2012) 075013, [[1207.1344](#)].
- [53] T. Corbett, O. J. P. Eboli, J. Gonzalez-Fraile and M. C. Gonzalez-Garcia, *Robust Determination of the Higgs Couplings: Power to the Data*, *Phys. Rev.* **D87** (2013) 015022, [[1211.4580](#)].
- [54] E. Massó and V. Sanz, *Limits on anomalous couplings of the Higgs boson to electroweak gauge bosons from LEP and the LHC*, *Phys. Rev.* **D87** (2013) 033001, [[1211.1320](#)].
- [55] B. Dumont, S. Fichet and G. von Gersdorff, *A Bayesian view of the Higgs sector with higher dimensional operators*, *JHEP* **07** (2013) 065, [[1304.3369](#)].

- [56] S. Banerjee, S. Mukhopadhyay and B. Mukhopadhyaya, *Higher dimensional operators and the LHC Higgs data: The role of modified kinematics*, *Phys. Rev.* **D89** (2014) 053010, [[1308.4860](#)].
- [57] J. Ellis, V. Sanz and T. You, *The Effective Standard Model after LHC Run I*, *JHEP* **03** (2015) 157, [[1410.7703](#)].
- [58] R. Edezhath, *Dimension-6 Operator Constraints from Boosted VBF Higgs*, [1501.00992](#).
- [59] T. Corbett, O. J. P. Eboli, D. Goncalves, J. Gonzalez-Fraile, T. Plehn and M. Rauch, *The Higgs Legacy of the LHC Run I*, *JHEP* **08** (2015) 156, [[1505.05516](#)].
- [60] A. Butter, O. J. P. Éboli, J. Gonzalez-Fraile, M. C. Gonzalez-Garcia, T. Plehn and M. Rauch, *The Gauge-Higgs Legacy of the LHC Run I*, [1604.03105](#).
- [61] J. J. Liu, C. S. Li, L. L. Yang and L. G. Jin, *Next-to-leading order QCD corrections to the direct top quark production via model-independent FCNC couplings at hadron colliders*, *Phys.Rev.* **D72** (2005) 074018, [[hep-ph/0508016](#)].
- [62] J. Gao, C. S. Li, J. J. Zhang and H. X. Zhu, *Next-to-leading order QCD corrections to the single top quark production via model-independent t - q - g flavor-changing neutral-current couplings at hadron colliders*, *Phys.Rev.* **D80** (2009) 114017, [[0910.4349](#)].
- [63] Y. Zhang, B. H. Li, C. S. Li, J. Gao and H. X. Zhu, *Next-to-leading order QCD corrections to the top quark associated with γ production via model-independent flavor-changing neutral-current couplings at hadron colliders*, *Phys.Rev.* **D83** (2011) 094003, [[1101.5346](#)].
- [64] B. H. Li, Y. Zhang, C. S. Li, J. Gao and H. X. Zhu, *Next-to-leading order QCD corrections to tZ associated production via the flavor-changing neutral-current couplings at hadron colliders*, *Phys.Rev.* **D83** (2011) 114049, [[1103.5122](#)].
- [65] Y. Wang, F. P. Huang, C. S. Li, B. H. Li, D. Y. Shao et al., *Constraints on flavor-changing neutral-current Htq couplings from the signal of tH associated production with QCD next-to-leading order accuracy at the LHC*, *Phys.Rev.* **D86** (2012) 094014, [[1208.2902](#)].
- [66] A. Buckley, C. Englert, J. Ferrando, D. J. Miller, L. Moore, M. Russell et al., *Global fit of top quark effective theory to data*, *Phys. Rev.* **D92** (2015) 091501, [[1506.08845](#)].
- [67] A. Buckley, C. Englert, J. Ferrando, D. J. Miller, L. Moore, M. Russell et al., *Constraining top quark effective theory in the LHC Run II era*, *JHEP* **04** (2016) 015, [[1512.03360](#)].
- [68] C. Degrande, J. M. Gerard, C. Grojean, F. Maltoni and G. Servant, *Probing Top-Higgs Non-Standard Interactions at the LHC*, *JHEP* **07** (2012) 036, [[1205.1065](#)].
- [69] N. Greiner, S. Willenbrock and C. Zhang, *Effective Field Theory for Nonstandard Top Quark Couplings*, *Phys. Lett.* **B704** (2011) 218–222, [[1104.3122](#)].
- [70] C. Zhang, N. Greiner and S. Willenbrock, *Constraints on Non-standard Top Quark Couplings*, *Phys. Rev.* **D86** (2012) 014024, [[1201.6670](#)].
- [71] H. Mebane, N. Greiner, C. Zhang and S. Willenbrock, *Effective Field Theory of Precision Electroweak Physics at One Loop*, *Phys. Lett.* **B724** (2013) 259–263, [[1304.1789](#)].
- [72] H. Mebane, N. Greiner, C. Zhang and S. Willenbrock, *Constraints on Electroweak Effective Operators at One Loop*, *Phys. Rev.* **D88** (2013) 015028, [[1306.3380](#)].
- [73] J. de Blas, M. Chala and J. Santiago, *Renormalization Group Constraints on New Top Interactions from Electroweak Precision Data*, *JHEP* **09** (2015) 189, [[1507.00757](#)].

- [74] J. Elias-Miró, C. Grojean, R. S. Gupta and D. Marzocca, *Scaling and tuning of EW and Higgs observables*, *JHEP* **05** (2014) 019, [[1312.2928](#)].
- [75] E. E. Jenkins, A. V. Manohar and M. Trott, *Renormalization Group Evolution of the Standard Model Dimension Six Operators I: Formalism and lambda Dependence*, *JHEP* **10** (2013) 087, [[1308.2627](#)].
- [76] E. E. Jenkins, A. V. Manohar and M. Trott, *Renormalization Group Evolution of the Standard Model Dimension Six Operators II: Yukawa Dependence*, *JHEP* **01** (2014) 035, [[1310.4838](#)].
- [77] R. Alonso, E. E. Jenkins, A. V. Manohar and M. Trott, *Renormalization Group Evolution of the Standard Model Dimension Six Operators III: Gauge Coupling Dependence and Phenomenology*, *JHEP* **04** (2014) 159, [[1312.2014](#)].
- [78] J. Alwall, R. Frederix, S. Frixione, V. Hirschi, F. Maltoni et al., *The automated computation of tree-level and next-to-leading order differential cross sections, and their matching to parton shower simulations*, *JHEP* **1407** (2014) 079, [[1405.0301](#)].
- [79] C. Zhang, *Automating Predictions for Standard Model Effective Field Theory in MadGraph5_aMC@NLO*, in *Proceedings, 12th International Symposium on Radiative Corrections (Radcor 2015) and LoopFest XIV (Radiative Corrections for the LHC and Future Colliders)*, 2016. [1601.03994](#).
- [80] G. Durieux, F. Maltoni and C. Zhang, *Global approach to top-quark flavor-changing interactions*, *Phys. Rev.* **D91** (2015) 074017, [[1412.7166](#)].
- [81] B. Gripaios, M. Nardecchia and T. You, *An Anomalous Composite Higgs and the 750 GeV Di-Gamma Resonance*, [1605.09647](#).
- [82] C. Grojean, E. Salvioni, M. Schlaffer and A. Weiler, *Very boosted Higgs in gluon fusion*, *JHEP* **05** (2014) 022, [[1312.3317](#)].
- [83] M. Buschmann, D. Goncalves, S. Kuttimalai, M. Schonherr, F. Krauss and T. Plehn, *Mass Effects in the Higgs-Gluon Coupling: Boosted vs Off-Shell Production*, *JHEP* **02** (2015) 038, [[1410.5806](#)].
- [84] A. Banfi, A. Martin and V. Sanz, *Probing top-partners in Higgs+jets*, *JHEP* **08** (2014) 053, [[1308.4771](#)].
- [85] Q.-H. Cao, B. Yan, D.-M. Zhang and H. Zhang, *Resolving the Degeneracy in Single Higgs Production with Higgs Pair Production*, *Phys. Lett.* **B752** (2016) 285–290, [[1508.06512](#)].
- [86] R. Contino, M. Ghezzi, M. Moretti, G. Panico, F. Piccinini and A. Wulzer, *Anomalous Couplings in Double Higgs Production*, *JHEP* **08** (2012) 154, [[1205.5444](#)].
- [87] F. Goertz, A. Papaefstathiou, L. L. Yang and J. Zurita, *Higgs boson pair production in the D=6 extension of the SM*, *JHEP* **04** (2015) 167, [[1410.3471](#)].
- [88] A. Azatov, R. Contino, G. Panico and M. Son, *Effective field theory analysis of double Higgs boson production via gluon fusion*, *Phys. Rev.* **D92** (2015) 035001, [[1502.00539](#)].
- [89] R. Grober, M. Muhlleitner, M. Spira and J. Streicher, *NLO QCD Corrections to Higgs Pair Production including Dimension-6 Operators*, *JHEP* **09** (2015) 092, [[1504.06577](#)].
- [90] C. Zhang and S. Willenbrock, *Effective-Field-Theory Approach to Top-Quark Production and Decay*, *Phys. Rev.* **D83** (2011) 034006, [[1008.3869](#)].

- [91] B. Grzadkowski, M. Iskrzynski, M. Misiak and J. Rosiek, *Dimension-Six Terms in the Standard Model Lagrangian*, *JHEP* **10** (2010) 085, [[1008.4884](#)].
- [92] M. Schulze and Y. Soreq, *Pinning down electroweak dipole operators of the top quark*, [1603.08911](#).
- [93] M. P. Rosello and M. Vos, *Constraints on four-fermion interactions from the $t\bar{t}$ charge asymmetry at hadron colliders*, *Eur. Phys. J.* **C76** (2016) 200, [[1512.07542](#)].
- [94] A. Alloul, N. D. Christensen, C. Degrande, C. Duhr and B. Fuks, *FeynRules 2.0 - A complete toolbox for tree-level phenomenology*, *Comput.Phys.Commun.* **185** (2014) 2250–2300, [[1310.1921](#)].
- [95] C. Degrande, C. Duhr, B. Fuks, D. Grellscheid, O. Mattelaer et al., *UFO - The Universal FeynRules Output*, *Comput.Phys.Commun.* **183** (2012) 1201–1214, [[1108.2040](#)].
- [96] C. Degrande, *Automatic evaluation of UV and R2 terms for beyond the Standard Model Lagrangians: a proof-of-principle*, *Comput. Phys. Commun.* **197** (2015) 239–262, [[1406.3030](#)].
- [97] V. Hirschi et al., *Automation of one-loop QCD corrections*, *JHEP* **05** (2011) 044, [[1103.0621](#)].
- [98] R. Frederix, S. Frixione, F. Maltoni and T. Stelzer, *Automation of next-to-leading order computations in QCD: The FKS subtraction*, *JHEP* **10** (2009) 003, [[0908.4272](#)].
- [99] V. Hirschi and O. Mattelaer, *Automated event generation for loop-induced processes*, *JHEP* **10** (2015) 146, [[1507.00020](#)].
- [100] T. Sjöstrand, S. Ask, J. R. Christiansen, R. Corke, N. Desai, P. Ilten et al., *An Introduction to PYTHIA 8.2*, *Comput. Phys. Commun.* **191** (2015) 159–177, [[1410.3012](#)].
- [101] M. Bahr et al., *Herwig++ Physics and Manual*, *Eur. Phys. J.* **C58** (2008) 639–707, [[0803.0883](#)].
- [102] S. Frixione and B. R. Webber, *Matching NLO QCD computations and parton shower simulations*, *JHEP* **06** (2002) 029, [[hep-ph/0204244](#)].
- [103] L. Berthier and M. Trott, *Towards consistent Electroweak Precision Data constraints in the SMEFT*, *JHEP* **05** (2015) 024, [[1502.02570](#)].
- [104] L. Berthier and M. Trott, *Consistent constraints on the Standard Model Effective Field Theory*, *JHEP* **02** (2016) 069, [[1508.05060](#)].
- [105] G. Passarino and M. Trott, *The Standard Model Effective Field Theory and Next to Leading Order*, Tech. Rep. LHCHXSWG-DRAFT-INT-2016-005, Mar, 2016.
- [106] R. Contino, A. Falkowski, F. Goertz, C. Grojean and F. Riva, *On the Validity of the Effective Field Theory Approach to SM Precision Tests*, [1604.06444](#).
- [107] R. Contino, A. Falkowski, F. Goertz, C. Grojean and F. Riva, *Comments on the validity of the Effective Field Theory approach to physics beyond the Standard Model*, Tech. Rep. LHCHXSWG-DRAFT-INT-2016-001, Mar, 2016.
- [108] L. A. Harland-Lang, A. D. Martin, P. Motylinski and R. S. Thorne, *Parton distributions in the LHC era: MMHT 2014 PDFs*, *Eur. Phys. J.* **C75** (2015) 204, [[1412.3989](#)].
- [109] P. Artoisenet, R. Frederix, O. Mattelaer and R. Rietkerk, *Automatic spin-entangled decays of heavy resonances in Monte Carlo simulations*, *JHEP* **03** (2013) 015, [[1212.3460](#)].

- [110] G. Passarino, *NLO Inspired Effective Lagrangians for Higgs Physics*, *Nucl. Phys.* **B868** (2013) 416–458, [[1209.5538](#)].
- [111] ATLAS collaboration, G. Aad et al., *Measurement of Higgs boson production in the diphoton decay channel in pp collisions at center-of-mass energies of 7 and 8 TeV with the ATLAS detector*, *Phys. Rev.* **D90** (2014) 112015, [[1408.7084](#)].
- [112] CMS collaboration, V. Khachatryan et al., *Observation of the diphoton decay of the Higgs boson and measurement of its properties*, *Eur. Phys. J.* **C74** (2014) 3076, [[1407.0558](#)].
- [113] CMS COLLABORATION collaboration, *First results on Higgs to gammagamma at 13 TeV*, Tech. Rep. CMS-PAS-HIG-15-005, CERN, Geneva, 2016.
- [114] ATLAS collaboration, G. Aad et al., *Observation and measurement of Higgs boson decays to WW^* with the ATLAS detector*, *Phys. Rev.* **D92** (2015) 012006, [[1412.2641](#)].
- [115] CMS collaboration, S. Chatrchyan et al., *Measurement of Higgs boson production and properties in the WW decay channel with leptonic final states*, *JHEP* **01** (2014) 096, [[1312.1129](#)].
- [116] ATLAS collaboration, G. Aad et al., *Measurements of Higgs boson production and couplings in the four-lepton channel in pp collisions at center-of-mass energies of 7 and 8 TeV with the ATLAS detector*, *Phys. Rev.* **D91** (2015) 012006, [[1408.5191](#)].
- [117] CMS collaboration, S. Chatrchyan et al., *Measurement of the properties of a Higgs boson in the four-lepton final state*, *Phys. Rev.* **D89** (2014) 092007, [[1312.5353](#)].
- [118] ATLAS collaboration, G. Aad et al., *Evidence for the Higgs-boson Yukawa coupling to tau leptons with the ATLAS detector*, *JHEP* **04** (2015) 117, [[1501.04943](#)].
- [119] CMS collaboration, S. Chatrchyan et al., *Evidence for the 125 GeV Higgs boson decaying to a pair of τ leptons*, *JHEP* **05** (2014) 104, [[1401.5041](#)].